Earth Systems and Environment (2026) 10:1961–1986
https://doi.org/10.1007/s41748-025-00726-8

ORIGINAL ARTICLE

Improving Real-Time Flood Forecasting: Probabilistic Validation of Assimilated Remotely-Sensed Soil Moisture Data

Samira Sadat Soltani[1,2] · **Alexandre Belleflamme**[1,2] · **Klaus Goergen**[1,2] · **Stefan Kollet**[1,2]

Received: 13 March 2025 / Revised: 7 July 2025 / Accepted: 10 July 2025 / Published online: 5 August 2025

Abstract

Precise hydrological modeling is crucial for effective water resource management, forecasting future water supply, and preparing for extreme events. The devastating July 2021 flood event over western Germany and eastern Belgium has raised concerns about the capacity of current models to predict such previously unrecorded extreme events. These concerns are intensified by the increasing frequency of extreme events linked to global warming. Modeling uncertainties highlight challenges in forecasting such events. To address these challenges, prognostic modeling techniques can be improved by incorporating satellite-derived soil moisture (SM) estimations into hydrological models. This has the potential to minimize uncertainty in soil moisture and streamflow simulations. In this study, the integrated hydrological model ParFlow-CLM was enhanced using an Ensemble Kalman Filter (EnKF) data assimilation (DA) technique. We used Sentinel-1-SM and ESA CCI (European Space Agency Climate Change Initiative)-SM data to improve the estimation of soil moisture and streamflow. We conducted the DA experiment over Germany and nearby regions in July 2021, using ParFlow-CLM with high spatial (611 m) and temporal (hourly) resolution. The key results are as follows: CCI-SM DA is a robust approach for representing soil moisture dynamics, outperforming both Sentinel-1-SM DA and open loop simulations without DA in terms of responsiveness and accuracy. This makes CCI-SM DA a better fit for high-resolution studies that depend on event-driven soil water content changes. Discharge from CCI-SM DA simulations provides the closest match to observed peak discharges, Sentinel-1-SM DA tends to slightly underpredict peak discharge at several locations, however still performs better than the open loop simulation.

✉ Samira Sadat Soltani
s.soltani@fz-juelich.de

[1] Institute of Bio- and Geosciences (IBG-3, Agrosphere), Forschungszentrum Jülich GmbH, 52425 Jülich, Germany

[2] Centre for High-Performance Scientific Computing in Terrestrial Systems, Geoverbund ABC/J, Jülich, Germany

Graphical Abstract

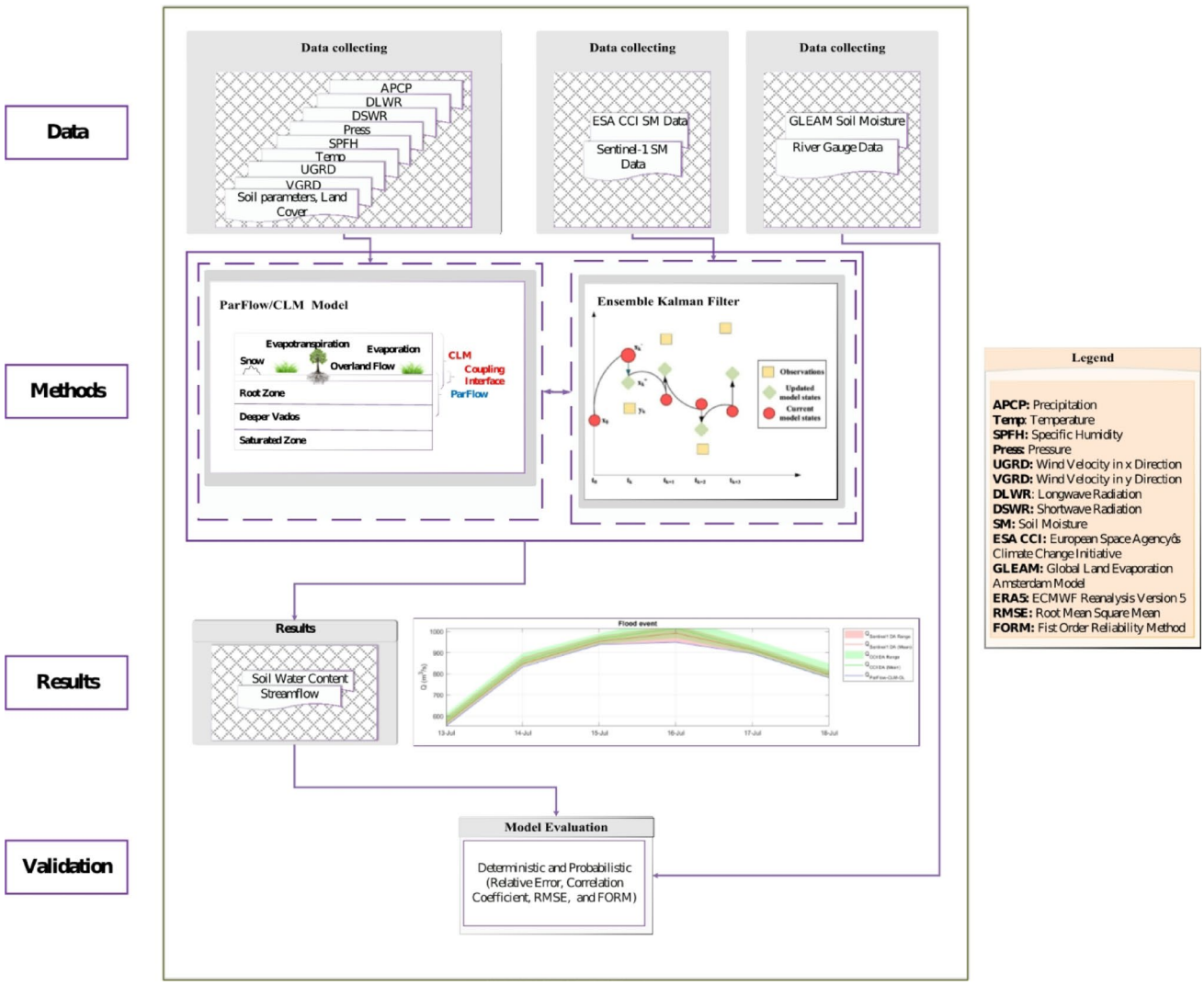

This graphical abstract presents a framework to enhance flood forecasting by assimilating satellite-derived soil moisture (SM) data into a physics-based hydrological ParFlow-CLM model. The methodology is applied to a real flood event in Germany, demonstrating its operational relevance for improving early warning systems. The core of the framework is the ParFlow-CLM integrated hydrologic model, which captures key surface and subsurface processes, including overland flow, evapotranspiration, snow accumulation, and 3D groundwater-surface water interactions. The model is driven by hourly atmospheric forcing data such as precipitation (APCP), temperature (Temp), specific humidity (SPFH), pressure (Press), wind speed (UGRD/VGRD), and longwave/shortwave radiation (DLWR/DSWR), primarily sourced from the ECMWF HRES medium-range forecast products. To improve model accuracy, soil moisture observations from ESA CCI (European Space Agency Climate Change Initiative), and Sentinel-1 are assimilated using the Ensemble Kalman Filter (EnKF). This sequential data assimilation method updates the model state by combining model forecasts with observational data, accounting for uncertainties in both. The EnKF propagates an ensemble of model states to estimate error statistics and correct the state variables based on incoming observations. Model outputs, including soil water content and streamflow, are evaluated against observations using deterministic and probabilistic performance metrics, such as relative error, *RMSE*, correlation coefficient, and the first order reliability method (FORM). The results show that incorporating SM data via EnKF significantly enhances the model's ability to predict flood peaks and soil moisture dynamics. This integrated approach is especially beneficial in flat or low-gradient terrains, where antecedent soil moisture conditions strongly influence runoff generation.

Highlights

- Soil moisture data assimilation in ParFlow-CLM improves flood prediction.
- EnKF with Sentinel-1 and ESA CCI soil moisture enhances streamflow simulations.
- ESA CCI data assimilation improves soil moisture accuracy.
- Data assimilation boosts extreme event forecasts in high-res sub-km, daily models.

Keywords Hydrologic Modeling · Model Evaluation · Soil Moisture · Extreme Flood Events · Data Assimilation · Ensemble Kalman Filter

1 Introduction

The ongoing warming of the climate increases the atmosphere's capacity to hold moisture, resulting in more frequent and intense summer rainfall events and a heightened risk of flash floods (Trenberth 2011; Lenderink and Van Meijgaard 2010; Westra et al. 2013; Myhre et al. 2019; Saadi et al. 2023a; Lenderink et al. 2025). These changes pose serious threats to infrastructure, ecosystems, and human life (Dottori et al. 2018; Nissen and Ulbrich 2017). The July 2021 flood in Germany caused over 180 deaths and EUR 46 billion in total damages, making it the country's costliest natural disaster (Munich Re, (Munich Re, 2022)).

Soil water content (SWC) plays a key role in regulating water, energy, and carbon exchanges between land and atmosphere, directly influencing runoff and flood intensity (Gebler et al. 2019; Brocca et al. 2009; Beck et al. 2009; Tramblay et al. 2010, 2011, 2012). Hydrological models estimate SWC and water partitioning, but their accuracy is limited by variable soil properties, land cover, topography, and rainfall patterns (Brocca et al. 2017).

Integrated terrestrial models (e.g., MikeShe, ParFlow-CLM, ParFlow/WRF, TSMP; Abbott et al. 1986; Maxwell and Miller 2005; Kollet and Maxwell 2006; Maxwell et al. 2011; Shrestha et al. 2014; Soltani et al. 2022a) simulate interactions between land surface and subsurface hydrology. Combined with in-situ data, they effectively capture SWC variability and its impact on rainfall-runoff dynamics (Cornelissen et al. 2014; Fatichi et al. 2015; Herbst et al. 2006; Ivanov et al. 2010; Soltani 2025). However, their high computational demands often limit parameter calibration and uncertainty assessment. Prognostic hydrological models can estimate variables such as soil moisture and streamflow but often struggle to meet the accuracy and reliability needs of flood management due to uncertainties in inputs, parameters, initial/boundary conditions, and model structure. Despite this, free-running models sometimes produce reasonably accurate results (Abbaszadeh et al. 2018; Matgen et al. 2010).

Recently, Data Assimilation (DA), based on Bayesian theory, has gained attention for integrating in-situ and remote hydrometeorological data into hydrological models to improve predictions and account for uncertainties (Reichle et al. 2002; Soltani et al. 2021). Various methods have been developed for incorporating soil moisture data, including sequential and variational approaches (Liu et al. 2012). The ensemble Kalman filter (EnKF), introduced by Evensen (1994) and (2003), is a widely used algorithm. By incorporating observations to update model states like soil moisture (Li et al. 2013; McMillan et al. 2013; Soltani et al. 2024) and snow water equivalent (Dechant and Moradkhani 2011; He et al., 2012), the EnKF improves streamflow forecasts. It can also update model states and parameters simultaneously (Moradkhani et al. 2005; Nie et al. 2011; Wang et al. 2009).

In this study, we aimed to close this gap of applying the EnKF on a complex high-resolution integrated hydrological model at the regional scale with 3-D heterogeneous fields of Mualem-van Genuchten subsurface parameters using real-world data. This study's methodology has three main focuses: first, assessing how catchment initial conditions, especially soil moisture, influence flood occurrence and magnitude; second, evaluating the ensemble Kalman filter (EnKF) for improving soil water content estimates and real-time flood forecasting; and third, proposing and applying the First Order Reliability Method (FORM; Madsen et al. 2006) to assess the failure probability of a Limit State Function (LSF) as a new way to validate data assimilation performance. To achieve these goals, we assimilated Sentinel-1 and CCI soil moisture data into the integrated ParFlow-CLM model over a flood-affected area in western Germany from July 2021. Results were validated using soil moisture from GLEAM and ERA5, along with river gauge observations. This study addresses key challenges in flood forecasting and risk assessment by combining advanced hydrological models with data assimilation techniques. We focus on the impact of initial soil conditions, evaluate state-of-the-art data assimilation methods, and apply probabilistic assessments of the FORM to improve flood prediction accuracy. Enhancing these forecasts is vital for better preparedness and mitigation amid rising flood risks from climate change. Specifically, we investigate whether catchment-scale hydrological characterization can be improved using high spatio-temporal resolution soil water content

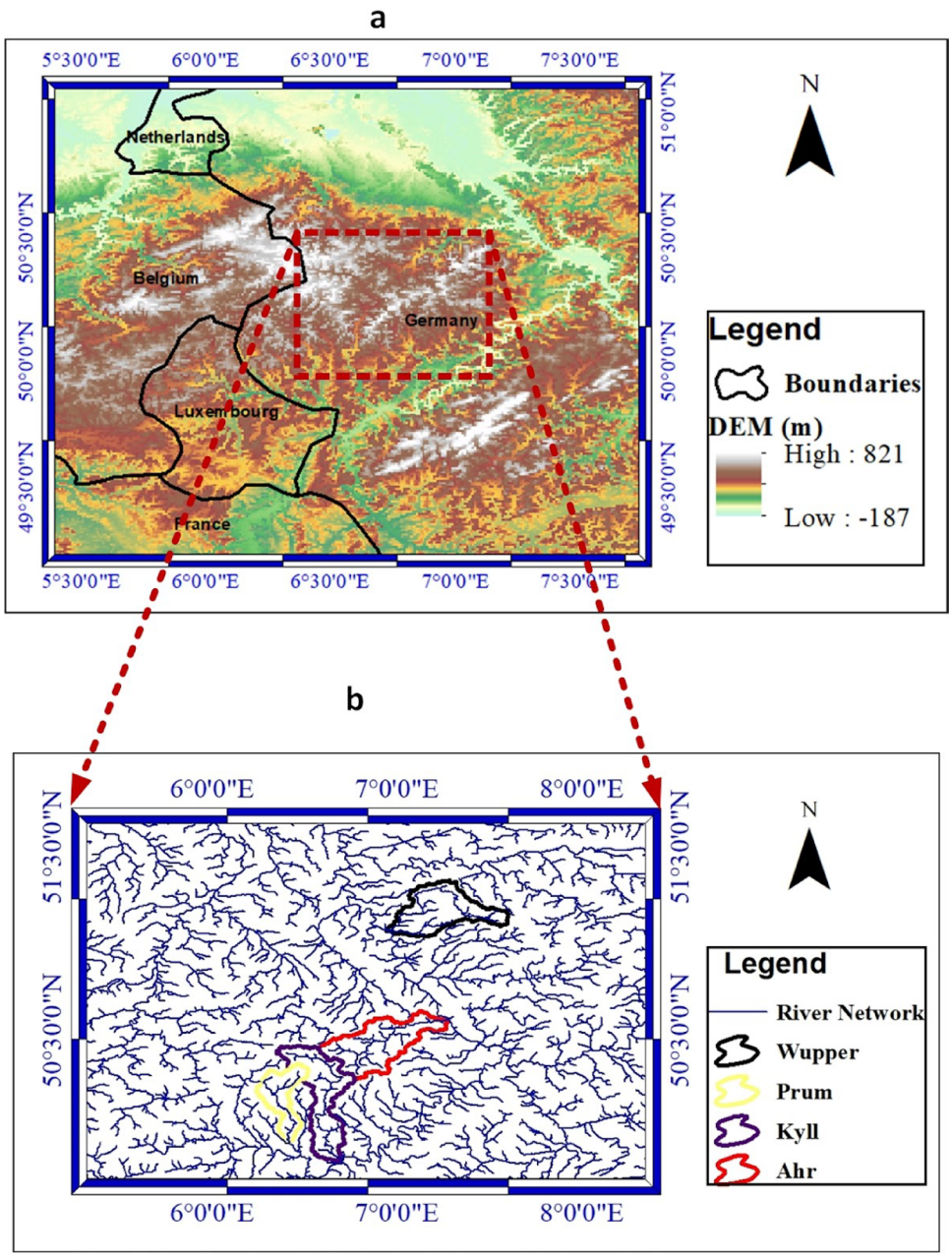

Fig. 1 (**a**) Overview map of the study area within Europe, overlaid with DEM from Global multi-resolution terrain elevation data 2010 (GMTED2010; Danielson and Gesch., 2011) (**b**) Map showing the river basins and related river networks

data through data assimilation. We also compare the performance of the ensemble Kalman filter (EnKF) by validating it against various soil moisture datasets, providing insights into its effectiveness across satellite-based, model-derived, and reanalysis data sources.

2 The July 2021 Flood in Western Europe

In July 2021, the Eifel-Ardennes region, characterized by its steep, deeply incised valleys, experienced severe flooding due to heavy rainfall. It is situated in southeast Belgium, Luxembourg, and western Germany (see Fig. 1a). It is bounded by the Meuse River to the west, the Moselle River to the south, and the Rhine River to the east. To the north, it extends into the Cologne Bay lowland region, Germany (see Fig. 1b). The affected region extends beyond the Eifel-Ardennes to the east, crossing the Rhine. Remarkably, the study area spans approximately 20,000 km^2 (150 × 130 km), an unusually large area considering the recorded high precipitation intensities and totals, which is a notable characteristic of this event according to Mohr et al. (2022). The study area is primarily covered by agricultural and forested landscapes, with only a minor fraction occupied by urban or built-up regions (see Fig. 2).

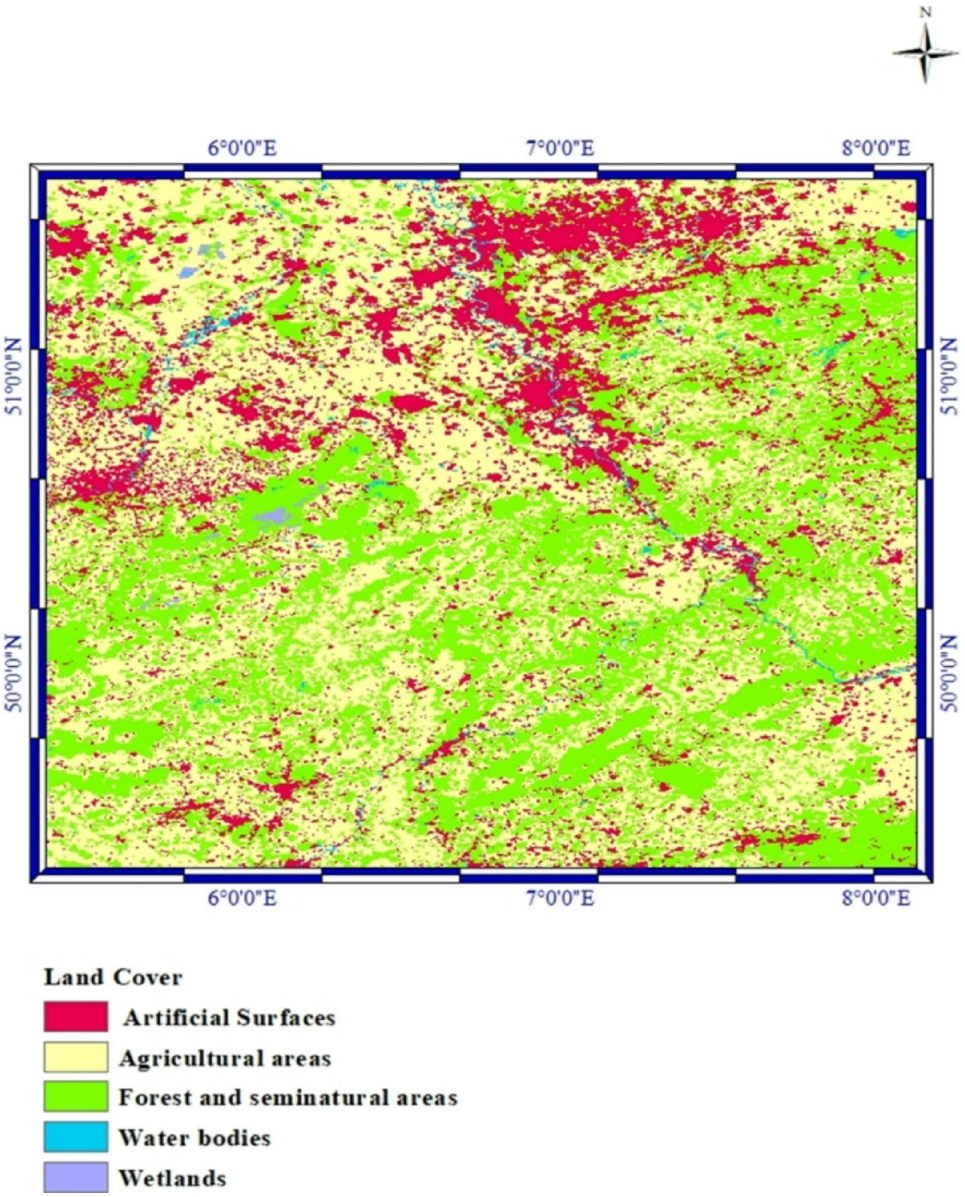

Fig. 2 The landscape characteristics across the domain using the CORINE Land Cover classification provided by the Copernicus Land Monitoring Service

In mid-July 2021, a cut-off low-pressure system named Bernd developed over central Europe, blocked by a stationary anticyclone in the northeast, creating conditions for heavy rainfall. Moisture-laden air masses, enriched by anomalously warm North and Baltic Seas, contributed significantly to the extreme precipitation. The synoptic setup, though not unprecedented, led to rare atmospheric moisture levels and intense rainfall over western Germany (Mohr et al. 2022. Annual precipitation levels vary between 700 and 1080 mm, while the aridity index falls from 0.5 to 0.9. These values indicate a temperate climate influenced by oceanic conditions, as described by Saadi et al. (2023a).

The July 2021 flood event in Western Europe was driven by intense and widespread precipitation, reaching up to 150 mm within 15 h on 14 July, with embedded convective activity. The event's spatial and temporal extent led to extreme return periods, exceeding 100–800 years in affected regions, highlighting its rarity. Precipitation significantly surpassed monthly climatological norms, emphasizing the event's exceptional hydro meteorological nature (Mohr et al. 2022.

Natural and anthropogenic landscape features, such as rock outcrops, tunnels, bridges, and mining pits, significantly influenced flood dynamics during the July 2021 event. These singularities caused unexpected flow diversions, erosion, and river course changes, as seen in Blessem and Altenahr, where infrastructure damage was severe (Dietze et al. 2022; Fekete and Sandholz 2021; BMI, (BMI 2022)). In some cases, such as the mining pit in Erftstadt,

they also served as unplanned retention basins, mitigating downstream flooding impacts.

2.1 Antecedent Conditions

Schröter et al. (2015) highlighted two primary causes in their analysis of Germany's significant historical floods: heavy rainfall after a period of normal or dry weather, and moderate rainfall following an unusually wet period. The moisture content of the catchment area before the event, particularly soil moisture levels, plays a critical role in the occurrence and intensity of floods. The Antecedent Precipitation Index (API; Kohler and Linsley (1951) for the 30 days before the event showed a wetter-than-usual period in much of Germany (Mohr et al. 2022). This finding is consistent with observations by Junghänel et al. (2021), who noted frequent rainfall three weeks before to the flood in the area, leading to high soil moisture levels. In areas such as the southern Eifel, the Ardennes in the northwest, and the Wupper region in the northeast, minimal soil moisture storage (less than 10 mm) was recorded (Mohr et al. 2022). Other regions had slightly higher soil moisture storage, typically ranging from 10 to 30 mm, with occasional peaks of 75 mm, but these levels remained below the average.

Similarly, Luxembourg experienced relatively moist antecedent conditions, as noted by AGE (2021). While the initial soil moisture was elevated but not unusually high, it contributed to flood formation through saturation excess. The intense rainfall further accelerated the transformation of rainfall into runoff by enhancing infiltration and generating overland flow, as reported by AGE (2021).

3 Methodology and Data

3.1 ParFlow-CLM Model

In this study, we utilized ParFlow-CLM, a sophisticated, parallel, and fully coupled subsurface-land surface model. This model effectively captures the complex dynamics of unsaturated and groundwater flow, as well as surface flow, within a comprehensive continuum framework (Maxwell et al. 2009; Kuffour et al. 2020). Water flow across 3-D variably saturated porous media is governed by the Richards equation, which ParFlow resolves (Ashby and Falgout 1996). For more details on the governing equations of the model, please refer to the Supplementary Material, section SM.1. Equations (Eqs. SM.1-SM.6) of the ParFlow-CLM.

ParFlow is a well-established, physics-based simulation platform widely used in various hydrological studies and applications (Frei et al. 2009; Kollet 2009; Maina et al. 2020; Soltani et al. 2022b, 2025). It has been applied to watershed hydrodynamics and hydrological scaling (Maxwell and Kollet 2008; Fang et al. 2015; Soltani 2022). This study uses the ParFlow-CLM setup described by Belleflamme et al. (2023). Previous work by Saadi et al. (2023a, b) explored the effects of radar-based precipitation products on streamflow simulation and flood nowcasting.

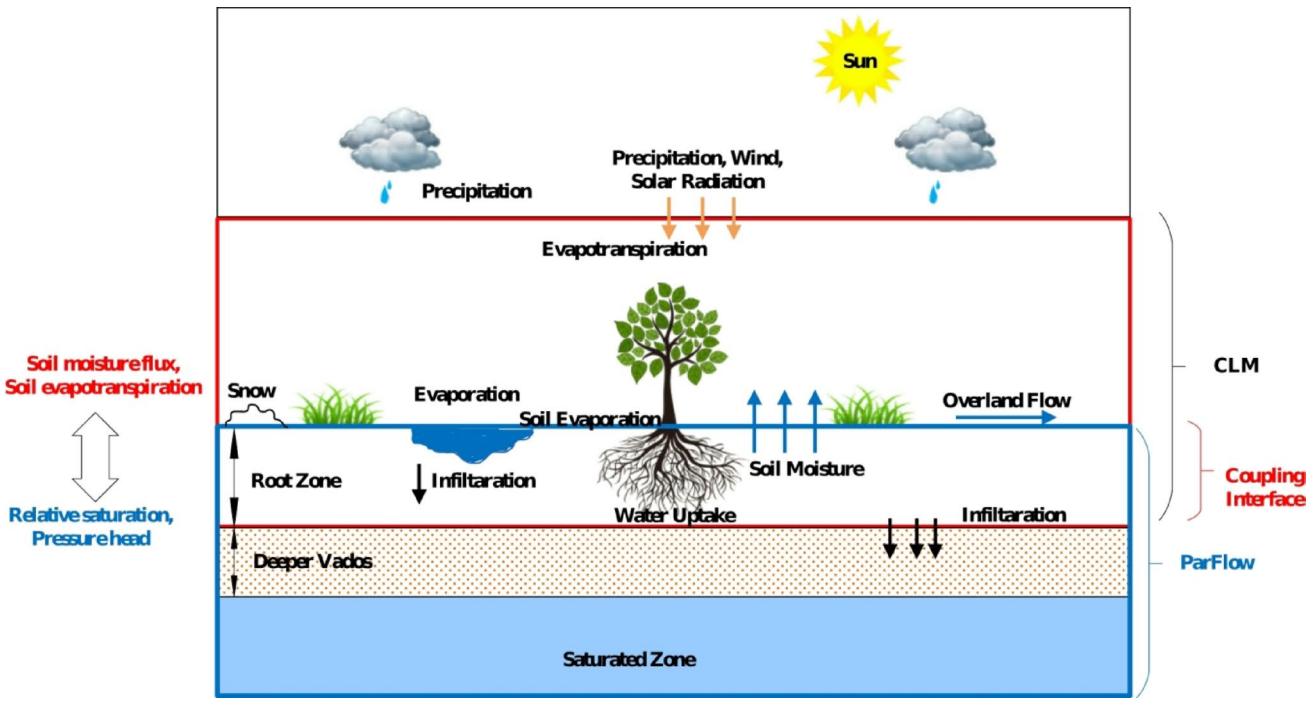

Fig. 3 Schematic of the coupled ParFlow-CLM model (Soltani 2022)

The Common Land Model (CLM), modified by Dai et al. (2003) and integrated into ParFlow (Kuffour et al. 2020), represents coupled water and energy exchanges between the subsurface and land surface, with atmospheric conditions as boundary inputs. Figure 3 illustrates the model setup, showing data exchange between CLM and ParFlow, especially in the root zone, including fluxes like infiltration and evapotranspiration, and state variables such as soil moisture and pressure head.

3.2 Data

3.2.1 Land Surface Data

ParFlow-CLM employs 18 land cover types defined by the International Geosphere-Biosphere Programme (IGBP), which are transformed into Plant Functional Types (PFTs) using various parameters. It utilizes the Europe-wide Corine Land Cover CLC2018 v20 dataset with a resolution of 100 m. Initially, the 44 land cover types from CLC2018 are translated into the 18 IGBP types, as described in Belleflamme et al. (2023).

3.2.2 Atmospheric Forcing

ParFlow-CLM requires eight atmospheric inputs: longwave and shortwave radiation, total precipitation, air temperature, air pressure, specific humidity, and wind components (Belleflamme et al. 2023). These are sourced from the ECMWF HRES medium-range forecast product at 0.1° resolution (~11 km) and downscaled to 0.0055° (~0.611 km) using bicubic interpolation to provide high-resolution, consistent inputs for the simulations.

3.2.3 Soil Types and Soil Hydraulic Parameters

ParFlow requires soil hydraulic parameters to solve water flow equations in variably saturated porous media. These parameters include porosity, saturated hydraulic conductivity, and parameters defining the Van Genuchten relationships. In Supplementary Material/Figure SM1, the soil texture of the upper layer was estimated based on SoilGrids250m data (Hengl et al. 2017), as described in Belleflamme et al. (2023).

3.2.4 Observational Data for DA

3.2.4.1 Sentinel-1 Soil Moisture Copernicus Land Monitoring Service provides Surface Soil Moisture, which represents the relative water content in the soil's upper few centimeters (https://land.copernicus.eu/en/products/soil-moisture). Surface soil moisture for the years 2014 to the present, these products are accessible in Europe at a resolution of 1 km (Bauer-Marschallinger et al. 2018).

3.2.4.2 ESA CCI Microwave Soil Moisture The European Space Agency's Climate Change Initiative (CCI) provides soil moisture (SM) data at a 0.25° spatial resolution. The latest CCI-SM version 08.1 (https://www.esaoilmoisture-cci.org) estimates soil moisture in the upper soil layers using microwave data from multiple satellite sensors (Dorigo et al. 2017). Passive microwave instruments include DMSP SSM/I, TRMM TMI, Aqua AMSR-E, Coriolis WindSat, SMOS, and SMAP, while active microwave data come from C-band scatterometers on ERS-1, ERS-2, and ASCAT A-B satellites (Wagner et al. 2013). Combining both active and passive datasets improves accuracy and reliability compared to using either alone (Liu et al. 2011).

3.2.5 Evaluation Data

3.2.5.1 GLEAM Products Global Land Evaporation Amsterdam Model (GLEAM) is a set of algorithms that estimate terrestrial evapotranspiration using parameterized physical processes, producing outputs like potential evaporation, surface soil moisture, and root zone soil moisture (Miralles et al. 2011). It relies on various remote sensing inputs, including vegetation optical depth, soil moisture, and snow-water equivalent. Root zone soil moisture is calculated using a multilayer running-water balance. In contrast with land models such as ERA5 and GLDAS, GLEAM bases its predictions on satellite data. GLEAM surface soil moisture products are publicly available at https://www.GLEAM.eu.

3.2.5.2 ERA5-Land ECMWF Reanalysis (ERA)5-Land is ECMWF's fifth-generation reanalysis dataset, providing global weather and climate data (Hersbach et al. 2020). It combines model outputs with observations using advanced 4D-var data assimilation, delivering hourly estimates for atmospheric, ocean-wave, and land-surface variables at a 0.025° (~30 km) resolution. ERA5 includes uncertainty estimates from a 10-member ensemble sampled every three hours. Soil moisture data is available at https://cds.climat

e.copernicus.eu/. All soil moisture datasets were upscaled to the coarsest grid to ensure consistent spatial resolution. Conservative first-order interpolation (Jones 1999) was used, applying weights based on overlapping areas between source and target grid cells. This method preserves fluxes of physical quantities during regridding.

3.2.5.3 River Gauge Data Water level (W) and streamflow (Q) data were collected from multiple river gauges across the study area, covering rivers from the Wupper in the east to the Amblève in the west. Gauges represented various basin sizes, ranging from 53.2 km² (Prüm 2/Prüm) to 816 km² (Kordel/Kyll), with efforts to include two gauges per rive, one in the headwaters and one near the junction. Water levels were measured directly, while streamflow was derived from water level data using gauge-specific W-Q relations. Where water level data were missing or invalid due to gauge damage or morphological changes, streamflow was estimated via hydraulic models or nearby gauges. Data were provided by local water authorities, including Rhineland-Palatinate and the Wupperverband (Mohr et al. 2022). Table 1 summarizes the gauge data.

3.3 Data Assimilation Framework

3.3.1 EnKF

In this study, the Ensemble Kalman Filter (EnKF) (Evensen 2003) was applied with the ParFlow-CLM model. EnKF is an ensemble-based, sequential data assimilation method that improves model state estimates by optimally combining model forecasts and observations. Figure SM2 provides a simplified schematic of the EnKF. The EnKF is widely used in hydrology due to its flexibility and ease of implementation (e.g., Naz et al. 2019; Gebler et al. 2019; Soltani 2022b).

The EnKF assimilation involves two main iterative steps: forecast and analysis. In the forecast step, multiple model simulations (50 ensemble members here) run forward in time with ParFlow-CLM. The ensemble size balances computational cost and accuracy, as larger ensembles better capture uncertainty but require more resources (Naz et al. 2019; Gebler et al. 2019; Soltani et al. 2024; Evensen 2003; Houtekamer and Mitchell 1998; Moradkhani et al. 2005; Reichle et al. 2002). This trade-off guides the choice of 50 members, reflecting both performance and efficiency considerations (Naz et al. 2019).

As detailed in Section SM1. Equations of ParFlow-CLM in supplementary material, the ParFlow-CLM model solves subsurface flow Eq. s (SM.1) and (SM.2) via the finite volume method and simulates overland flow. Variations in stochastic realizations arise from uncertainties in initial conditions and precipitation inputs. The forecast step (as Eq. 1) follows:

$$x_i^{f,t} = M(x_i^{t-1}, q_i^t) \tag{1}$$

The predicted model state vector at t time step t, is defined as $x_i^{f,t}$ while $x_i^{t-1}$is used as the model state vector from the prior time step t-1. The model forcings, $q_i^t$for each ensemble realization i (where i ranges from 1 to 50) are incorporated into the process. In the ParFlow model, one of the key prognostic variables is SWC. The model state vector $x_i^{f,t}$contains the simulated SWC values for various grid cells (as Eq. 2). In this study, Θ observations are assimilated:

Table 1 Essential attributes of river basins and measurement gauges, including water level (W) and streamflow (Q), are examined. The term HQ100 refers to a flood event with a statistical return period of 100 years. The peak factor is calculated as the maximum streamflow (Q) in 2021 divided by HQ100. This analysis also encompasses historical extreme statistics and the July 2021 flood event, with values for the latter being approximate estimates

		Previous historical extreme		Statistical extreme	Flood event in July 2021				
Gauge name	Basin size (km^2)	Max. W (cm)	Max. Q (m^3/s^{-1})	HQ_{100} (m^3/s^{-1})	Peak time (UTC)	Max. W (cm)	Max. Q (m^3/s^{-1})	Peak factor (-)	Operator and data provider
Ahr river basin									www.lfu.rlp.de
Altenahr	749.0	371	236	241	15 July 00:00	984–1019	1000	4	
Kyll river basin									www.lfu.rlp.de
Jünkerath	175.6	266	129	118	14 July 22:45	370	200	1.7	
Kordel	816.3	481	218	248	15 July 08:30	600	600	2.5	
Prüm river basin									www.lfu.rlp.de
Prüm 2	53.2	126	43.5	51.6	14 July 21:15	330	120	2.3	
Prümzurlay	576.1	492	252	278	15 July 05:30	700	600	2	
Wupper river basin									www.wupperverband.de
Opladen	606	306	219	250	15 July 02:45	460	530	2.1	

$$y_i{}^t = \theta_i{}^t + \varepsilon_i \tag{2}$$

where $y_i{}^t$ is the observation vector and ε_i is a vector, whose elements contain random values drawn from a uniform distribution. The SWC values in the model state vector are updated (as Eq. 3) by incorporating the Θ observations:

$$x_i^{a,t} = x_i^{f,t} + K^t \left[y_i^t - h x_i^{f,t} \right] \tag{3}$$

The updated state vector is represented here as $x_i{}^{a,t}$, with K denoting the Kalman gain and $y_i{}^t$the observation vector. The measurement operator h is nonlinear and manages the transformation between the measured SWC and the simulated SWC. The updated SWC is then converted to pressure head using the Mualem–van Genuchten relationship, as described by Reichle et al. (2002) and Gebler et al. (2019). This is how the Kalman gain K is calculated as Eq. 4:

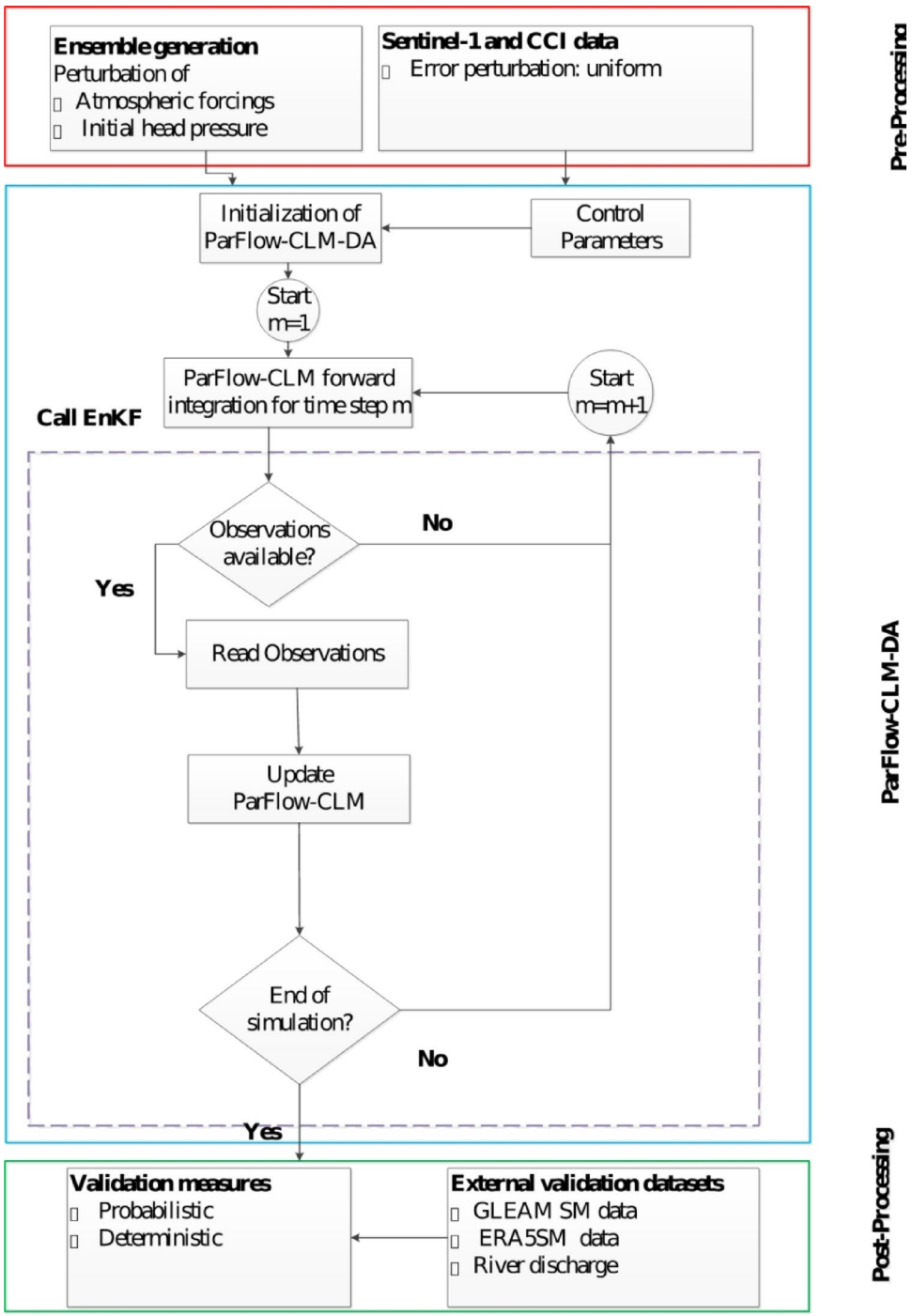

Fig. 4 An outline of the data assimilation process that includes (i) the pre-processing of the model input and observations, (ii) the ParFlow-CLM-DA, and (iii) the final processing step to assess the performance of the DA (modified from Soltani et al. 2024).

$$K^t = Cov(x_i^{f,t}, y_i^{f,t})(Cov(y_i^{f,t}, yi^{f,t}) + R)^{-1} \quad (4)$$

Cov represents covariance, and R is the observation error covariance matrix with soil water content (SWC) measurement error variances on its diagonal. The data assimilation framework requires a filter algorithm, observation files, and input ensembles (see Fig. 4). Pre-processing includes preparing soil moisture data, error estimates, and input ensembles. Post-processing compares ParFlow-CLM outputs against independent datasets for evaluation using cross-validation with GLEAM and ERA5, as illustrated in Fig. 4.

3.3.2 ParFlow-CLM-DA Experimental Design

Assimilation tests were conducted from June 1 to July 31, 2021, using ParFlow-CLM at a 611 m spatial resolution with hourly time steps and daily assimilation windows. Flood frequency and intensity are strongly influenced by catchment conditions, especially soil wetness (AGE, 2021). Sentinel-1 and CCI soil moisture data were assimilated starting 30 days before the flood event and continuing a few days after, covering the rainy period indicated by the Antecedent Precipitation Index.

A uniform observational error of 0.04 m^3/m^3 was applied to soil moisture data, consistent with reported uncertainties in ESA CCI and Sentinel-1 products (Colliander et al. 2017; Lievens et al. 2017; Dorigo et al. 2017; Bauer-Marschallinger et al. 2018). To address uncertainties in atmospheric forcing and initial conditions, precipitation and initial pressure were perturbed using geographically uniform, log-normal multiplicative factors with a mean of 1.0 and standard deviation of 0.10 (Naz et al. 2019; Soltani et al. 2024). Initial pressure included random noise with a 10% standard deviation. The ensemble size for both precipitation and pressure perturbations was set to 50 to update soil water content and pressure head across the domain.

3.4 Validation Strategy

3.4.1 Deterministic Assessment

To evaluate model performance in simulating hydrological variables, we use Relative Error (*RE*; Eq. 5) (Willmott 1981), Correlation Coefficient (*R*; Eq. 6) (Legates and McCabe 1999), Root Mean Squared Error (*RMSE*; Eq. 7) (Moriasi et al. 2007; Chai and Draxler 2014), Coefficient of Efficiency (*CE*; Eq. 8) (Nash and Sutcliffe 1970), and a probabilistic reliability assessment (detailed later). *RMSE* quantifies overall error magnitude, *RE* normalizes errors for comparison across catchments, and *CE* combines correlation, bias, and variability for a comprehensive measure of predictive skill. Together, these metrics provide a robust evaluation of the model's accuracy from both deterministic and probabilistic perspectives. The formulas for these metrics are as follows:

$$\mathrm{RE}_t = \frac{|{y_{obs}}^t - \hat{y}^t|}{{y_{obs}}^t} \quad (5)$$

$$R = \frac{\sum_{t=1}^{n} ({y_{obs}}^t - \bar{y})(\hat{y}^t - \overline{\hat{y}^t})}{\sqrt{\sum_{t=1}^{n} ({y_{obs}}^t - \bar{y})^2 \sum_{t=1}^{n} (\hat{y}^t - \overline{\hat{y}^t})^2}} \quad (6)$$

$$RMSE = \frac{\sqrt{\sum_{t=1}^{n} ({y_{obs}}^t - \hat{y}^t)^2}}{n} \quad (7)$$

RE serves as a means to categorize the percentage of samples into three groups: "low *RE*" with *RE*<15%, "medium *RE*" with 15% < *RE*<35%, and "high *RE*" with *RE*>35%, as delineated by Corzo and Solomatine (2007).

$$CE = 1 - \frac{\sum_{t=1}^{n} (y_{obs}^t - \hat{y}^t)^2}{\sum_{t=1}^{n} (y_{obs}^t - \bar{y})^2} \quad (8)$$

CE evaluates model performance relative to the mean of observed data, ranging from 1 (perfect fit) to negative values. Negative *CE* means the model performs worse than simply using the observed mean. *CE* is equivalent to *R* in linear regression. It is considered a better goodness-of-fit measure than the coefficient of determination (Willmott 1981; Legates and McCabe 1999; Harmel and Smith 2007). Moriasi et al. (2007) proposed a grading system: *CE*<0.50 is unsatisfactory, 0.50–0.65 satisfactory, 0.65–0.75 good, and 0.75–1.00 very good.

Since many recent studies found out that the DA Accuracy (*DAA*; Eq. 9) is between 5% and 25% of corresponding average precipitation (Long et al. 2014; Sahoo et al. 2011). We assumed that the accuracy of DA strategies would be less than 20% of corresponding average precipitation (P^t) as following (Soltani et al. 2024):

$$DAA = \frac{|{y_{obs}}^t - \hat{y}^t|}{\frac{1}{n}\sum_{t=1}^{n} P^t} \quad (9)$$

3.4.2 Probabilistic Assessment: the First order Reliability Method

The First Order Reliability Method (FORM), outlined by Madsen et al. (2006), is commonly used to assess system reliability in fields like structural, geotechnical, and hydrological engineering (Soltani et al. 2020, 2024). FORM estimates the probability that soil moisture or river stage exceeds critical thresholds, signaling flood risk. It models uncertain inputs (e.g., precipitation), transforms them into standardized normal variables, and uses linear approximations to efficiently calculate failure probabilities.

In this method, the Limit State Function (LSF) is key to approximating system failure. FORM transforms random variables into a standard Gaussian space and then uses a first-order Taylor series expansion at the design point to linearly approximate the LSF as Eq. 10 (Rackwitz and Fiessler 1979).

$$G(y) = L(y) = G(y_m) + \nabla G(y_m)^T.(y - y_m) \tag{10}$$

where G(y) is the failure function of a hydrologic system, L(y) is the LSF linearization,$y = (y_1, y_2, ..., y_n)$is the vector of n variables in G(y) function, ym is the expansion point, and$\nabla G$is the first order gradient vector of G(y).

In this study, FORM is used to assess the accuracy of DA experiments via different LSFs. The failure function G(y) defined as follows in Eq. 11(Corzo and Solomatine 2007), Eq. 12 (Moriasi et al. 2007) and Eq. 13 (Long et al. 2014; Sahoo et al. 2011; Soltani et al. 2024):

$$G(y) = 0.35 < RE \tag{11}$$

$$G(y) = 0.75 > CE \tag{12}$$

$$G(y) = DAA > 0.2 \tag{13}$$

The design point refers to the location within the transformed space of the failure domain that has the highest probability density. It is determined by solving an optimization problem. Specifically, the Hasofer-Lind-Rackwitz-Fiessler (HLRF; Liu and Der Kiureghian 1991) algorithm, an iterative gradient-based method, is used for this type of reliability analysis (Papaioannou and Straub 2021; see Fig. 5). The reliability index is defined as the shortest distance between the design point and the failure surface as Eq. 14 (Madsen et al. 2006):

$$\beta = \|y^*\| \tag{14}$$

The failure probability of G(y), representing the accuracy of predictions, can be approximated using the reliability index β once it has been determined as Eq. 15 (Madsen et al. 2006):

$$P_f = \Phi(-\beta) \tag{15}$$

where$\Phi(-\beta)$is the standard normal variates cumulative distribution. A smaller value of P_f corresponds to reduced uncertainty in the accuracy of predictions, showing heightened accuracy of the DA experiment's reliability. Figure 5 outlines the steps involved in the FORM. This systematic approach provides a computationally efficient way to assess the reliability of complicated systems (Soltani et al. 2020).

4 Results

4.1 Impact of DA on SWC Estimates

Figure 6 illustrates the simulated and observed SWC (m^3 m^{-3}) at six locations during the SWC ESA CCI Data Assimilation experiment period, alongside daily precipitation totals. The upper panels show SWC evolution, while the lower panels present precipitation as a driving input. This figure evaluates the performance of different modeling approaches: ParFlow-CLM-OL (open loop) simulations (without assimilation) and SWC ESA CCI assimilation scenario, with the GLEAM dataset.

The assimilation of SWC ESA CCI data improves alignment with observed SWC trends, particularly during high-precipitation periods in mid-July. Open loop simulations consistently underestimate SWC in most locations, while assimilation better captures the buildup and response of soil moisture to rainfall events. For example, at several locations (e.g., Altenahr-Ahr and Jünkerath-Kyll), assimilation effectively reflects pre-flood saturation, unlike open loop simulations.

Significant precipitation in mid-July (14–15 July), coupled with already high SWC levels at multiple sites, underscores the critical role of antecedent soil moisture in amplifying runoff and flooding. Locations such as Prümzurlay-Prüm and Opladen-Wupper show that assimilation produces smoother, more realistic SWC patterns compared to open loop simulations, which deviate significantly during wetter periods.

Overall, incorporating SWC ESA CCI data enhances the model's ability to reproduce observed SWC dynamics, particularly under extreme rainfall conditions. This highlights the importance of antecedent soil moisture conditions in understanding and predicting flood risks.

Figure 7 shows the spatial distribution of SWC during a flood event, comparing two DA scenarios, observational and model-based products, and an open loop simulation. ESA

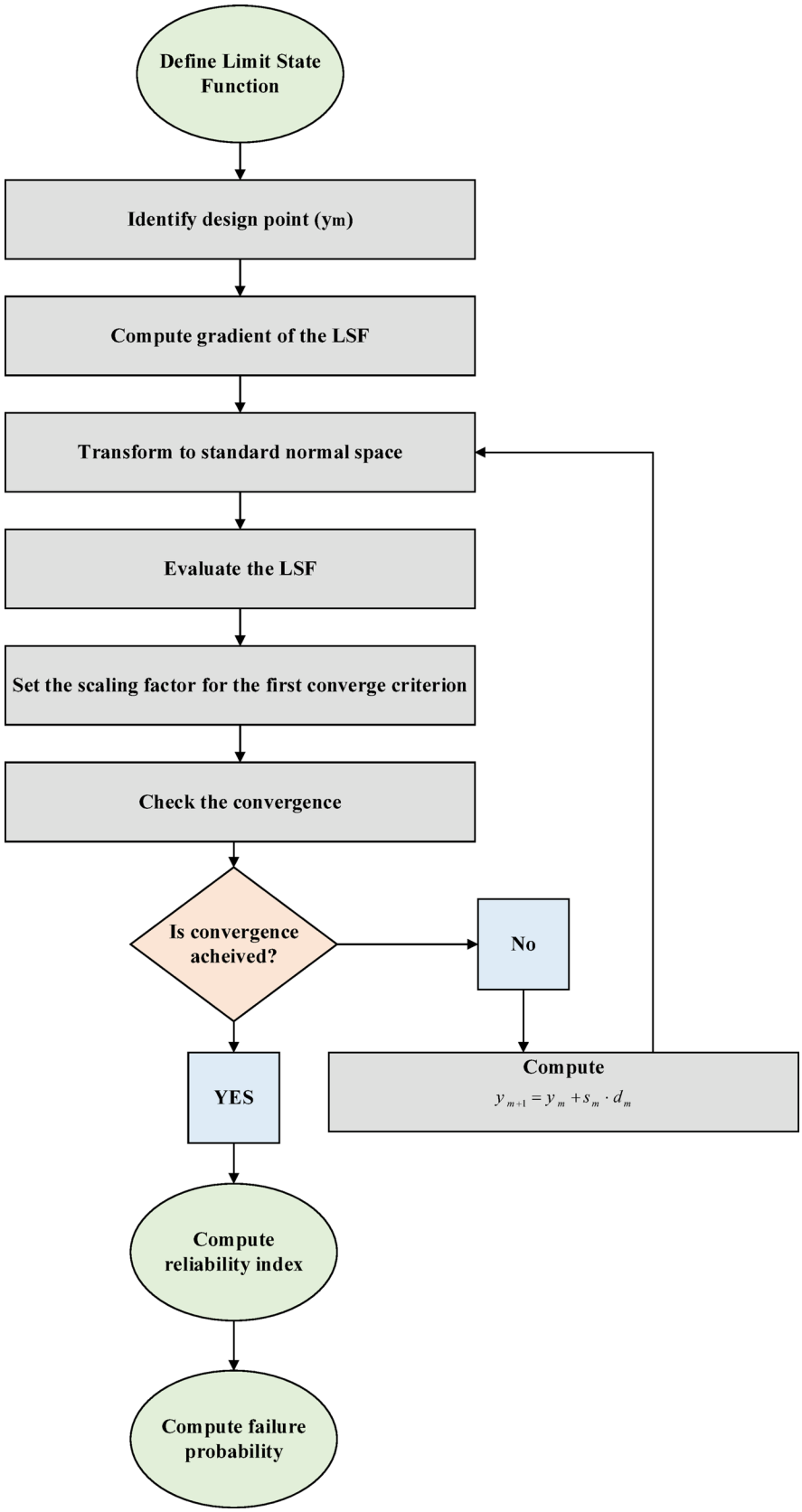

Fig. 5 Flowchart illustrates the sequential steps of the First Order Reliability Method (FORM), including defining LSF, identifying the design point, computing the gradient of the LSF, transforming variables to standard normal space, computing the reliability index, and estimating the failure probability (Modified from Soltani et al. 2020).

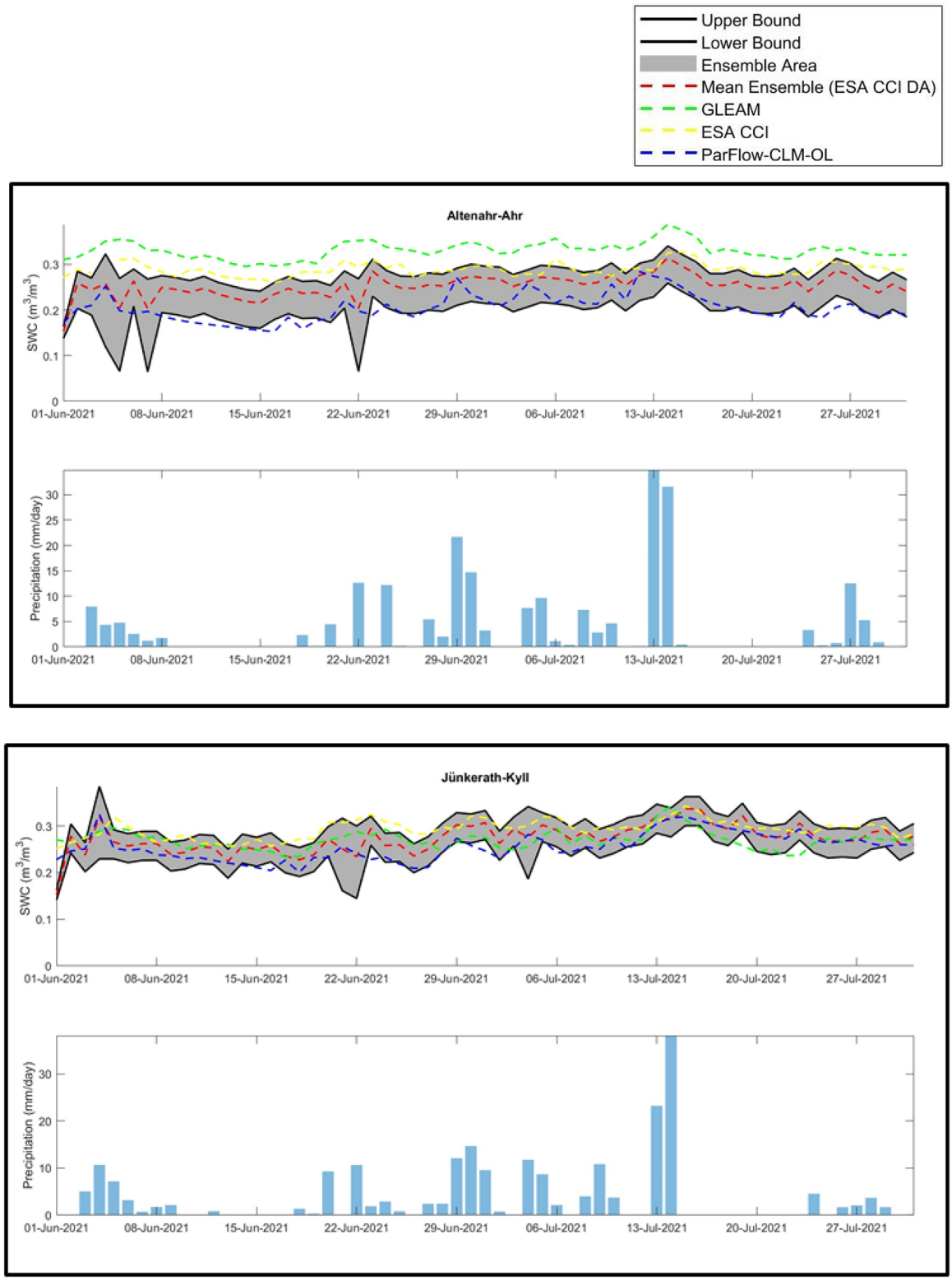

Fig. 6 Simulated and observed SWC (m^3 m^{-3} (upper panels)) during SWC CCI DA experiments period at individual locations: Altenahr-Ahr, Jünkerath-Kyll, Kordel-Kyll, Prüm2-Prüm, Prümzurlay-Prüm, and Opladen-Wupper. GLEAM data are indicated as evaluation datasets. Open loop (ParFlow-CLM-OL) simulations are shown alongside different updating scenarios for comparison. Precipitation is also indicated daily (bottom panels). The black lines represent the upper and lower uncertainty bounds, while the shaded gray area indicates the ensemble spread. The red dashed line represents the mean ensemble from the ESA CCI DA experiment. Green, yellow, and blue dashed lines correspond to GLEAM, ESA CCI, and ParFlow-CLM-OL datasets, respectively, providing additional comparative references

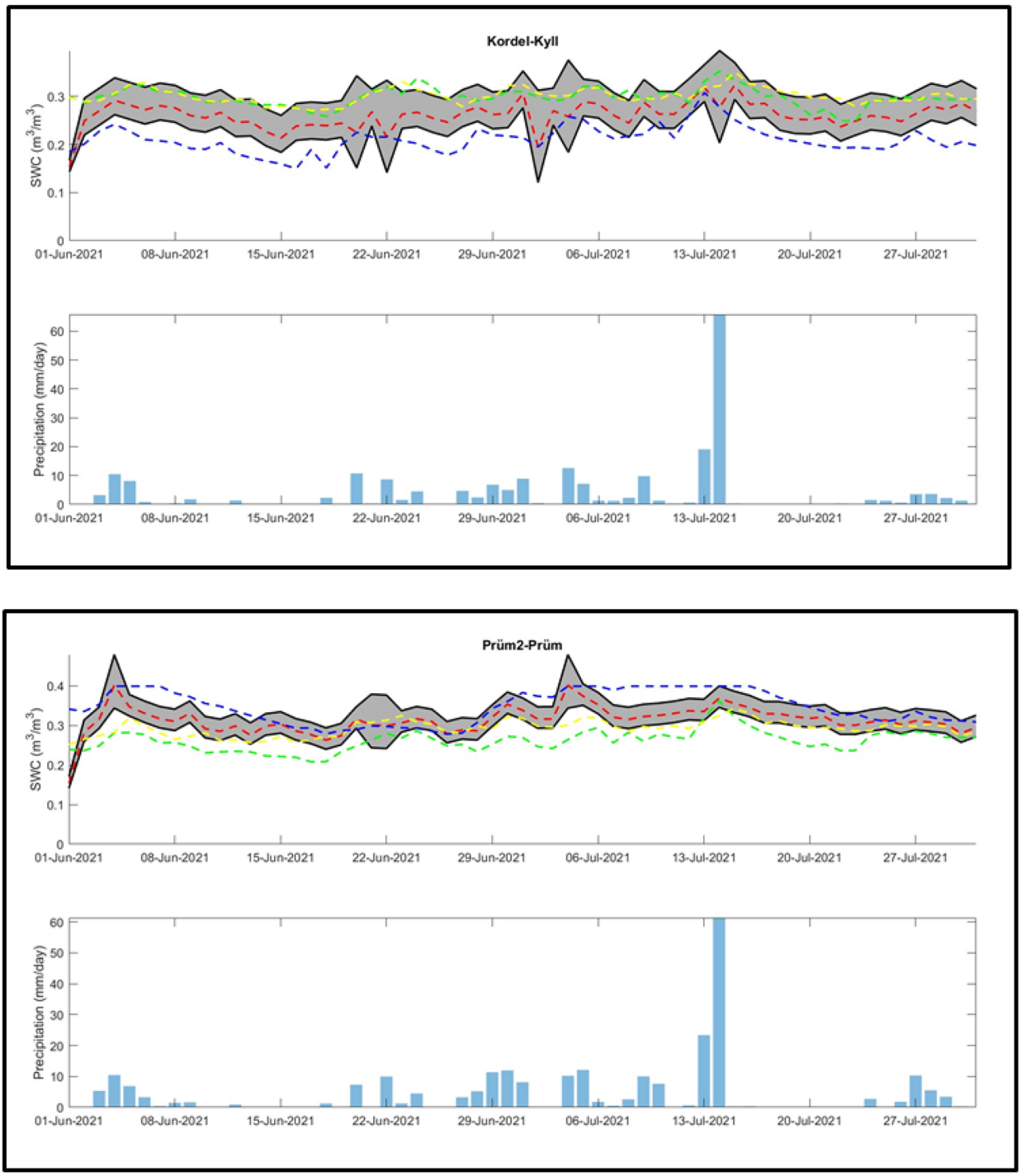

Fig. 6 (continued)

CCI-DA aligns closely with the GLEAM dataset, capturing regional trends and smoother transitions in soil moisture. Sentinel-1-DA captures finer spatial details but has lower overall agreement with GLEAM. It is worth noting that, due to the methodological similarities and overlapping input datasets between the GLEAM model and the ESA CCI soil moisture product, the assimilation of ESA CCI-SM yields simulated SWC that more closely aligns with GLEAM-derived SWC, in comparison to results obtained from Sentinel-1 SM assimilation.

This study has some limitations. The spatial resolution mismatch between datasets, SM-Sentinel-1 (1 km), CCI (0.25° or 27 km), and the model (611 m), can impact result evaluation. To address this, we resampled the SM data to

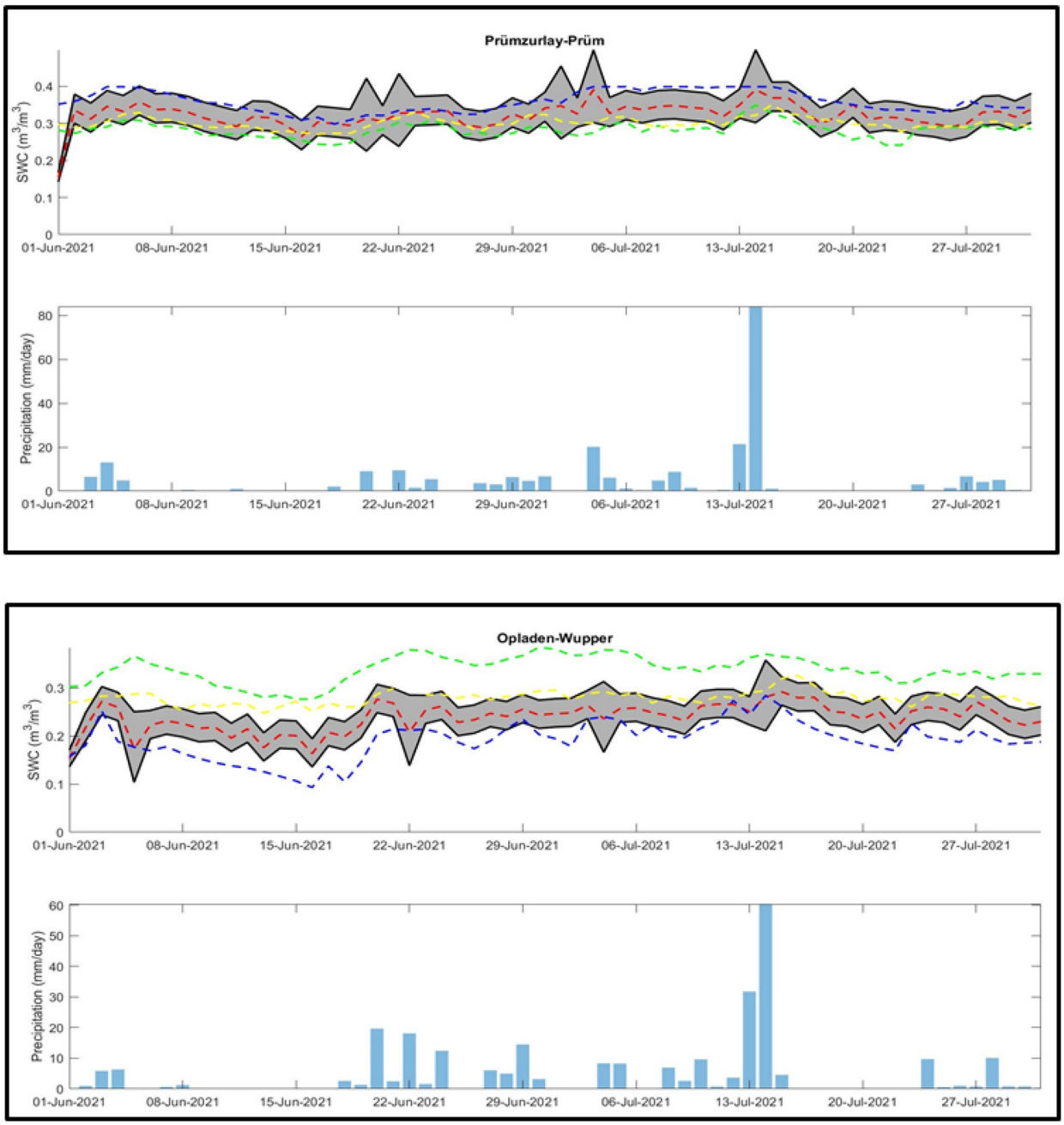

Fig. 6 (continued)

611 m using the First-Order Conservative method, preserving data integrity. Additionally, we applied multiple perturbation methods to account for precipitation errors, as these can significantly affect model performance. Understanding errors in both input and observational data enhances the accuracy and reliability of the results.

4.2 SWC Validation: Deterministic Assessment

Figure 8 evaluates the performance of SWC Sentinel-1-DA, ESA CCI-DA, ParFlow-CLM-OL, and ERA5 by visualizing their *RE* compared to the GLEAM dataset, which is used as the evaluation reference. *RE* is lowest for ESA CCI-DA, which demonstrates values close to or below 0.2 across most of the region, indicating strong agreement with GLEAM. Sentinel-1-DA shows slightly higher errors, with *RE* ranging between 0.2 and 0.3 in large areas, though it still improves

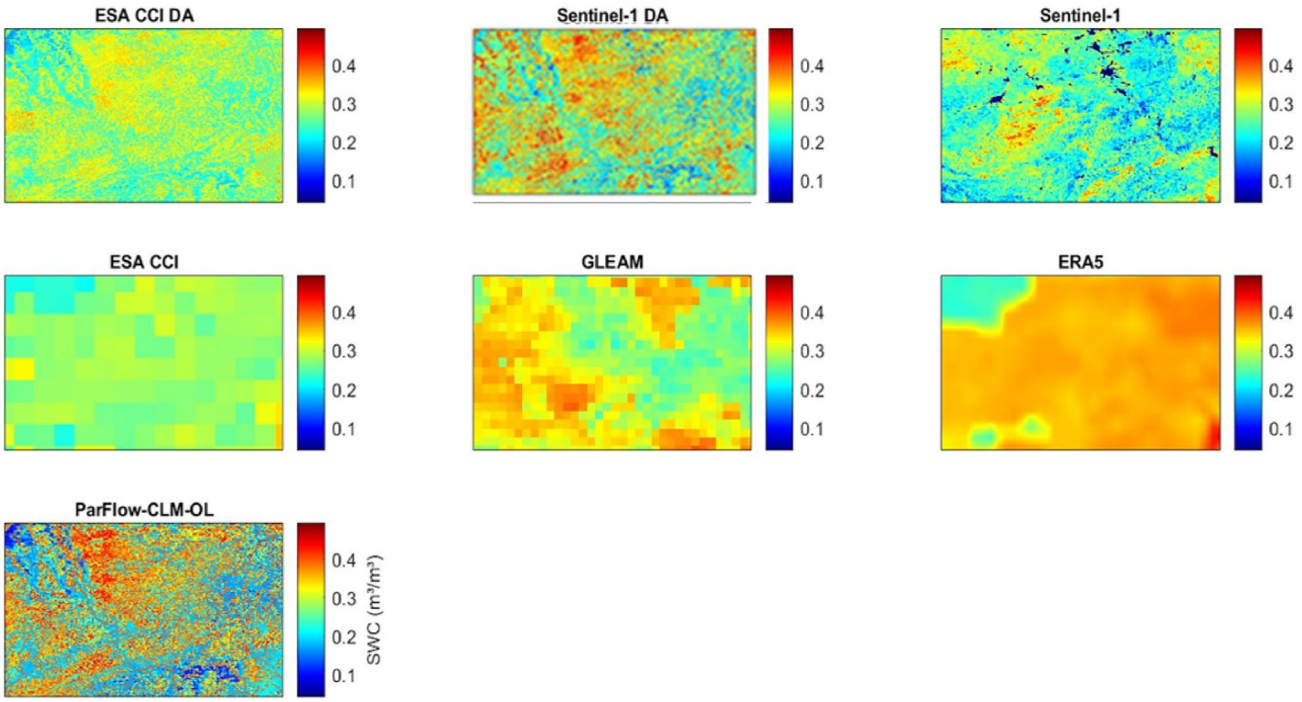

Fig. 7 Temporally averaged SWC (in m^3 m^{-3}) over the flood period (14–15 th July) for ESA CCI-DA, Sentinel-1-DA, Sentinel-1, ESA CCI, GLEAM, ERA5, ParFlow-CLM-OL

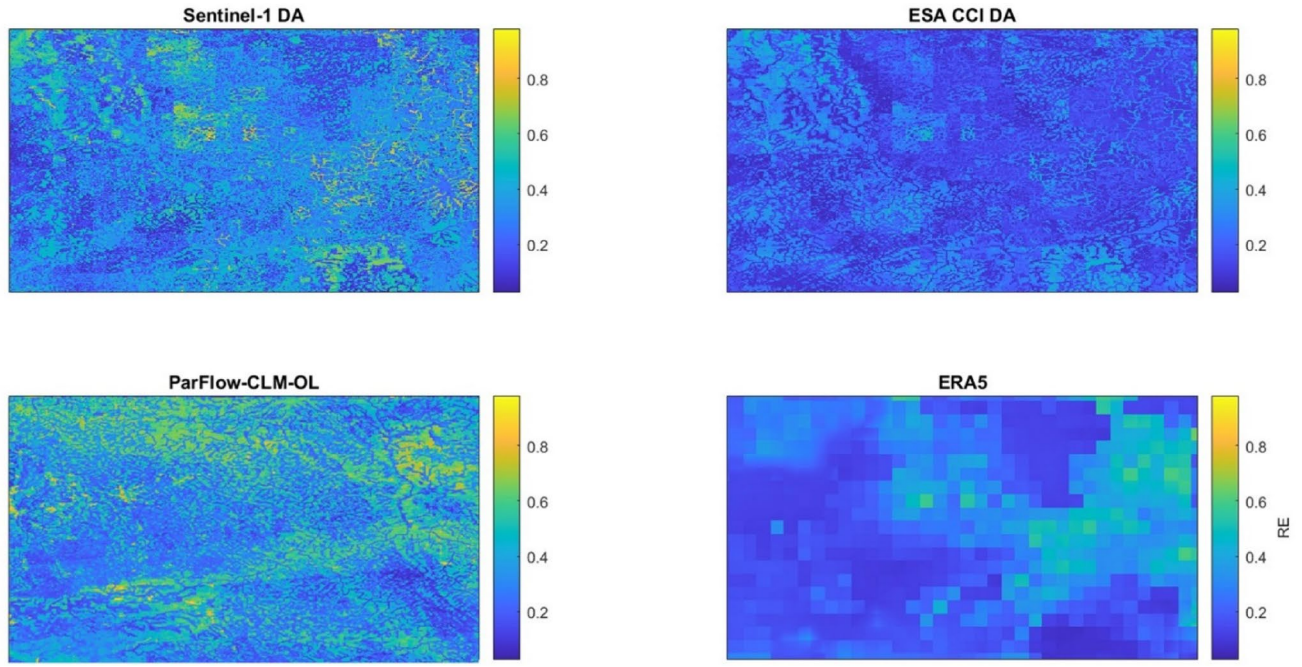

Fig. 8 RE (as a ratio between 0 and 1) of SWC between Sentinel-1-DA, ESA CCI-DA, ParFlow-CLM-OL, ERA5 and GLEAM

slightly compared to the open loop (ParFlow-CLM-OL) simulation. ParFlow-CLM-OL exhibits *RE* values exceeding 0.4–0.5 in many regions, highlighting the impact of not incorporating observational data. ERA5 performs the worst, with large areas exceeding 0.5 *RE* and a lack of fine spatial detail, reflecting its limitations as a model-only product. Comparatively, the assimilation of ESA CCI data reduces the error more effectively than Sentinel-1 data, making ESA CCI-DA the best-performing dataset in terms of *RE* reduction against GLEAM. It is worth noting that the strong

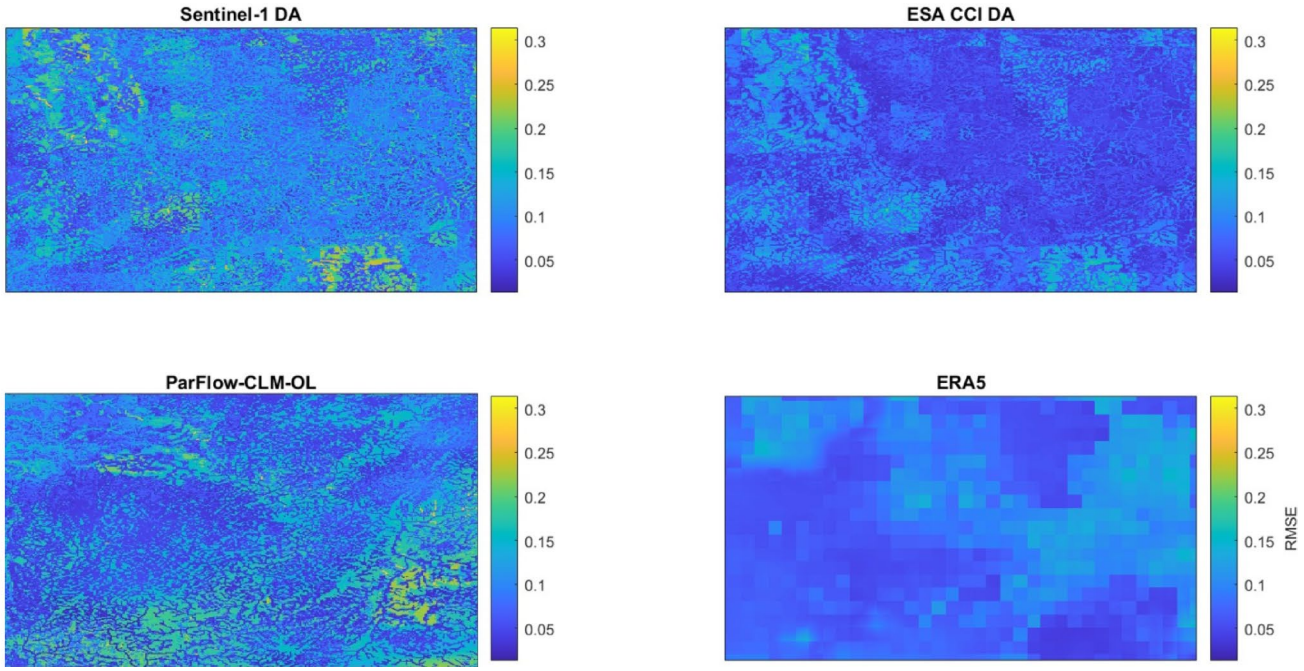

Fig. 9 RMSE of SWC between Sentinel-1-DA, ESA CCI-DA, ParFlow-CLM-OL, ERA 5 and GLEAM

performance of ESA CCI data assimilation was anticipated, as GLEAM is derived from ESA CCI data through its use of key satellite-based variables, such as soil moisture and vegetation optical depth, which are integral components of the GLEAM model.

Figure 9 presents RMSE of SWC for four datasets; Sentinel-1 DA, ESA CCI DA, ParFlow-CLM-OL, and ERA5, when compared to the GLEAM dataset. The RMSE ranges from 0.05 (dark blue, indicating lower error) to 0.3 (yellow, indicating higher error). Sentinel-1 DA shows predominantly low RMSE values, indicating errors in the range of 0.05–0.1, although some localized patches exhibit higher errors (up to 0.3). ParFlow-CLM-OL exhibits somewhat higher RMSE values than Sentinel-1 DA, with more frequent areas of intermediate errors and a slightly broader range of values, though still largely within the 0.05–0.15 range. ESA CCI DA also shows predominantly low RMSE values, comparable to Sentinel-1 DA, with most regions falling in the 0.05–0.1 range, indicating strong alignment with GLEAM. In contrast, ERA5 shows generally higher RMSE values, with substantial areas falling in the range of 0.1–0.15.

The performance improvements achieved through soil moisture data assimilation in this study are consistent with findings from previous research. For example, Naz et al. (2019) and Tian et al. (2020) reported similar reductions in *RMSE* and *RE* when assimilating ESA CCI soil moisture, especially in regions with high antecedent wetness. Our observed *RE* values for ESA CCI DA (<0.2) align well with their results.

Figure 10 compares the spatial correlations of SWC between different datasets and approaches and GLEAM. Both data assimilation experiments (CCI DA and Sentinel-1 DA) improve spatial correlations compared to the open loop run (ParFlow-CLM-OL). Sentinel-1 DA generally shows better correlations in certain regions, suggesting that its higher resolution enhances the model's representation of SWC. The open loop run shows lower correlations, reflecting the model's limitations without observational data. ERA5, with its coarser resolution, provides smoother patterns but serves as a useful benchmark for comparing the data assimilation methods.

4.3 SWC Validation: Probabilistic Assessment

Table 2 presents the probability of failure (P_f) estimates derived using the FORM, with the limit state function (LSF) defining the boundary between safe and failure conditions, as outlined in Sect. 3.4.2. The analysis incorporates three critical metrics: the reliability index ($RE > 0.35$), the consistency efficiency ($CE < 0.75$), and the deterministic design accuracy ($DAA > 0.2$), which are used to assess the reliability and performance of the model across different scenarios.

The results indicate that data assimilation reduces the probability of failure compared to the open loop model. Specifically, the Sentinel-1 DA and CCI DA scenarios show lower probabilities of failure across all three metrics. For instance, the probability of failure for the Sentinel-1 DA experiment is 18%, 17%, and 14% for the three metrics, respectively, while the CCI DA scenario shows even lower

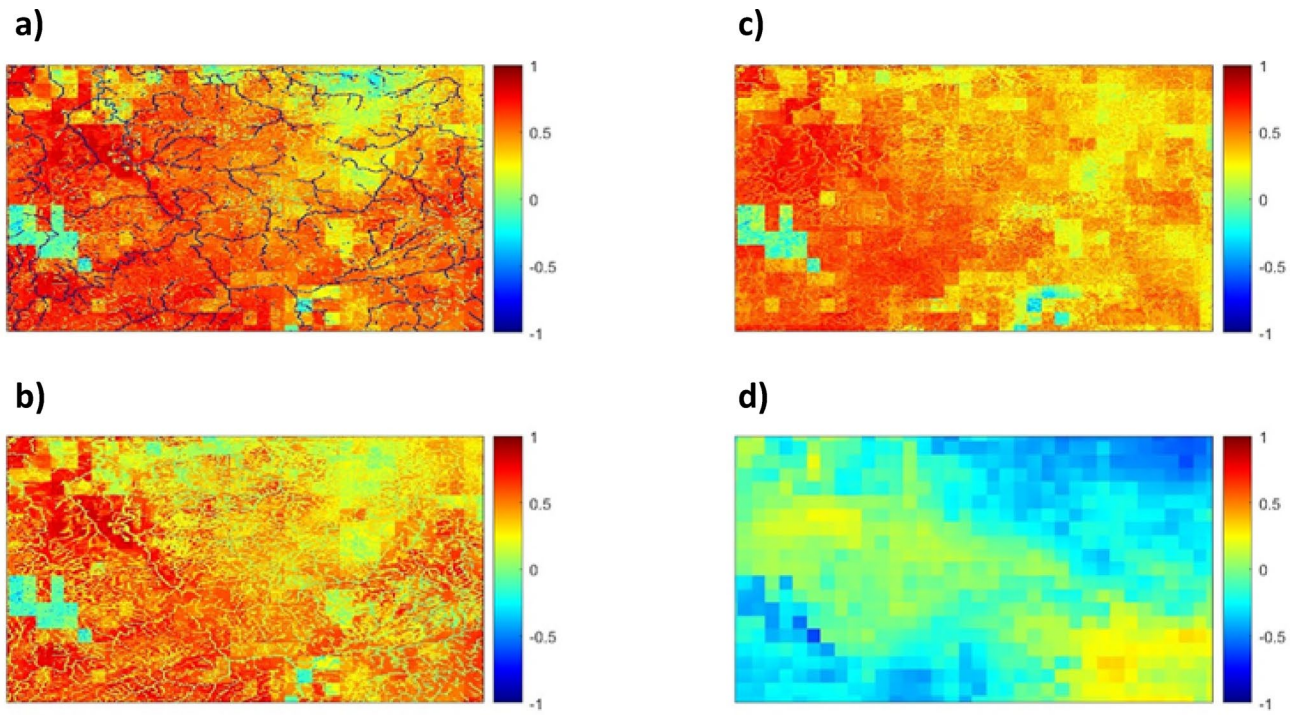

Fig. 10 Spatially correlation of SWC for (**a**) Sentinel-1-DA, (**b**) ParFlow-CLM-OL, (**c**) ESA CCI-DA, (**d**) ERA 5 and GLEAM

Table 2 The probability of failure calculated using the FORM. The analysis is based on three key metrics: *RE* greater than 0.35, *CE* less than 0.75, and *DAA* greater than 0.2

	P_f		
	LSF (refer to 3.4.2 section)		
	$RE > 0.35$	$CE < 0.75$	$DAA > 0.2$
Sentinel-1-DA	18%	17%	14%
ESA CCI-DA	9%	10%	8%
Open loop	24%	25%	22%

probabilities of failure at 9%, 10%, and 8%. In contrast, the open loop model, which does not use any data assimilation, shows substantially higher probabilities of failure: 24%, 25%, and 22%.

These findings suggest that incorporating data assimilation techniques, such as Sentinel-1 DA and CCI DA, improves the model's performance by reducing the probability of failure. This decrease in P_f reflects a more accurate and reliable model, with data assimilation helping to correct model biases and uncertainties. The reduction in failure probability means that the model's predictions are more aligned with observed conditions, enhancing the confidence in its ability to represent the system's behavior under varying environmental conditions.

The overall improvement demonstrated by the data assimilation experiments highlights the importance of integrating observational data into hydrological models. By reducing P_f, data assimilation contributes to the model's reliability and predictive accuracy, ultimately improving decision-making in water resource management and risk assessment. Thus, data assimilation serves as a powerful tool for enhancing model performance, especially in complex systems where uncertainties are inherent, leading to more robust and trustworthy predictions.

The probabilistic validation using FORM in this study provides a more rigorous assessment of failure risk than typically reported. Most earlier studies, such as Santis et al. (2021), focused on deterministic metrics, whereas our P_f estimates (as low as 8–10% for ESA CCI DA) indicate a stronger reduction in failure risk.

4.4 Impact of DA on Discharge Estimates

Figure 11 displays both simulated (left panels) and observed (in blue, right panels) discharge at multiple locations during the assimilation period, with a particular focus on the flood event from July 14–15, 2021. Overall, the $Q_{\text{CCI DA}}$ and $Q_{\text{Sentinel-1 DA}}$ updating scenarios show notable improvements over the open loop simulations in terms of accurately capturing the peak discharge values observed during the flood. In all locations, the simulation scenarios with data assimilation using ESA CCI and Sentinel-1 (green and red ranges/means) demonstrate an improved match to observed discharge, particularly in capturing the Q_{peak}, compared to the open loop (ParFlow-CLM-OL, blue line in right panels).

Table 3 provides the peak discharge values (Q Peak, in m^3/s) and RE (%) for simulations conducted with and

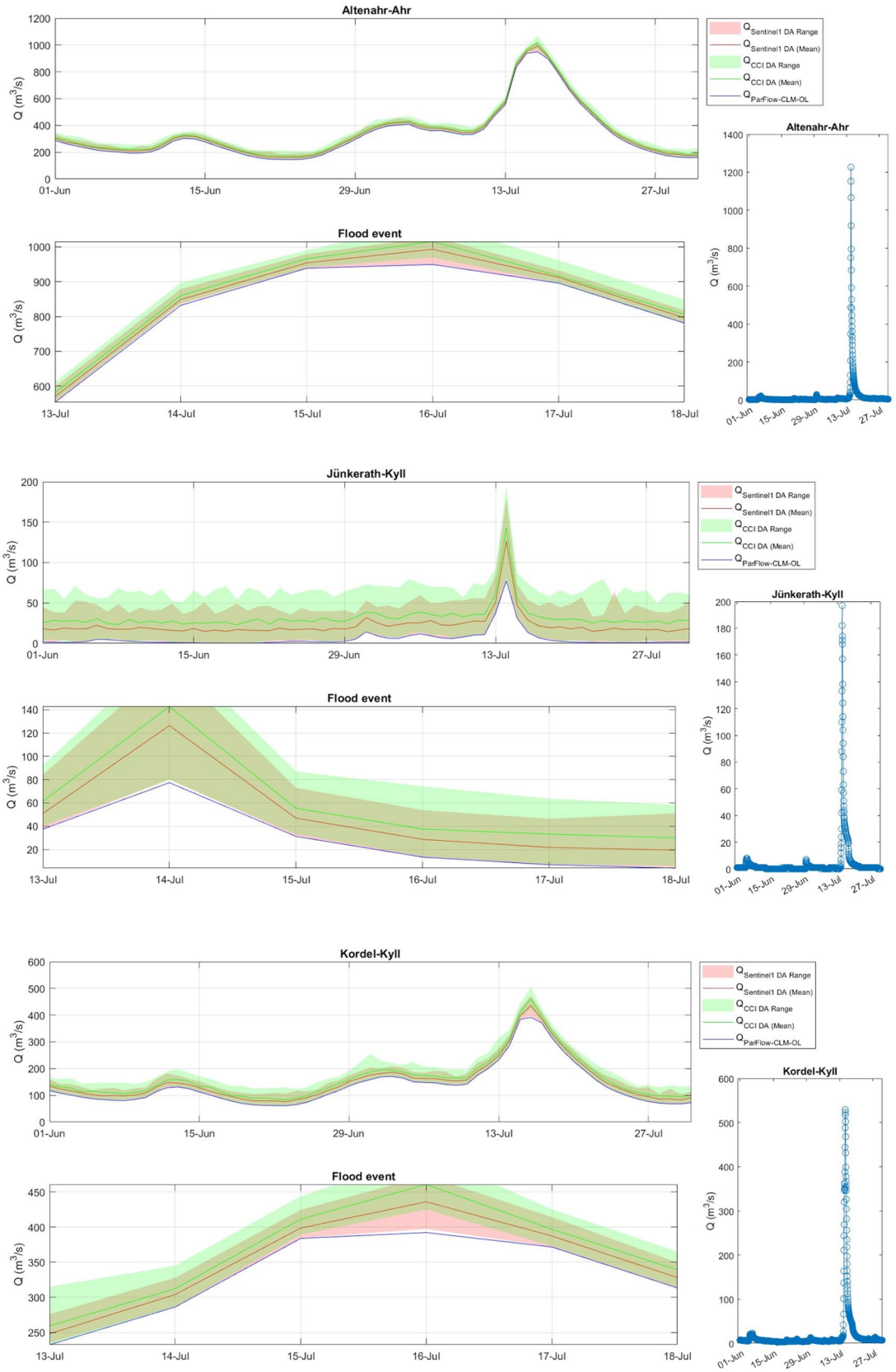

Fig. 11 Simulated (left panels) and observed hourly discharge (right panels) during the assimilation period at individual locations: (a) Altenahr-Ahr, (b) Jünkerath-Kyll, (c) Kordel-Kyll, (d) Prüm2-Prüm, (e) Prümzurlay-Prüm, and (f) Opladen-Wupper. The flood event period (July 14–15, 2021) is highlighted. ParFlow-CLM-OL simulation is shown alongside data assimilation scenarios for comparison

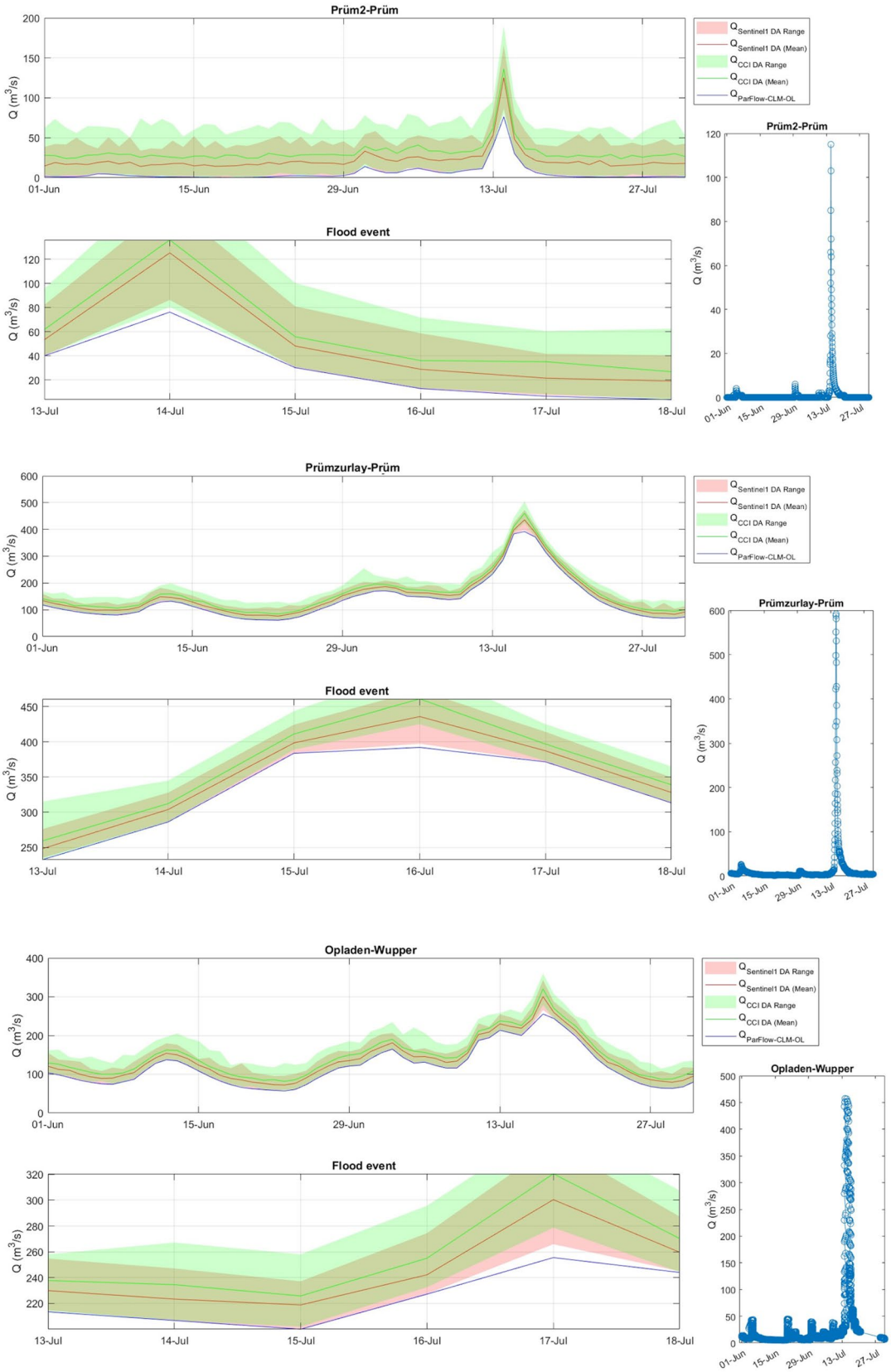

Fig. 11 (continued)

Table 3 Maximum Q and *RE* (refer to eq. 11; observed Q_{Peak} is based on table 1) of simulated Q with data assimilation (ESA CCI and Sentinel-1) compared to open loop (ParFlow-CLM-OL) across locations: (a) Altenahr-Ahr, (b) Jünkerath-Kyll, (c) Kordel-Kyll, (d) Prüm2-Prüm, (e) Prümzurlay-Prüm, and (f) Opladen-Wupper

	Q_{Peak} (m^3/s)						RE (%)					
	(a)	(b)	(c)	(d)	(e)	(f)	(a)	(b)	(c)	(d)	(e)	(f)
Sentinel-1-DA	969	122	425	125	420	300	3.1	39	29	8.3	30	43
ESA CCI DA	1015	142	460	130	450	320	1.5	29	23	4.1	25	39
ParFlow-CLM-OL	949	77	392	76	380	225	5.1	61	34	36	36	51

without data assimilation (DA) using ESA CCI and Sentinel-1 data in the ParFlow-CLM model, evaluated across various locations (a–f). The open loop simulation (ParFlow-CLM-OL), which does not include data assimilation, is also included for comparison. The results clear-ly demonstrate that the assimilation of ESA CCI and Sentinel-1 data consistently reduces RE compared to the open loop simulation, highlighting the improved accuracy of the model when satellite-based data are incorporated

For instance, at location (a), the *RE* decreases from 5.1% in the open loop to 3.1% with Sentinel-1 DA and further to 1.5% with ESA CCI DA. This trend is observed across all locations, with ESA CCI consistently achieving the lowest *RE*, followed by Sentinel-1. At location (f), the *RE* drops from 51% in the open loop to 43% with Sentinel-1 DA and to 39% with ESA CCI DA, further emphasizing the superior performance of ESA CCI in improving simulation accuracy.

Additionally, the simulated peak discharge values with data assimilation align more closely with observed peak discharge values (as shown in Table 1), particularly when using ESA CCI. In contrast, the open loop simulations exhibit the highest *RE* across all locations, such as at location (d), where the error is 36% compared to 8.3% for Sentinel-1 DA and 4.1% for ESA CCI DA. These findings underscore the limitations of the open loop approach and demonstrate the effectiveness of satellite data assimilation in enhancing the reliability of flood simulations in the ParFlow-CLM model.

4.5 Probabilistic Discharge Validation

Table 4 presents the probability of failure (P_f) calculated using the First-Order Reliability Method (FORM) for six locations under the condition that Data Assimilation Accuracy (DAA) > 0.2. Sentinel-1-DA, ESA CCI-DA, and ParFlow-CLM-OL are compared to assess hydrological risks, such as flooding, at individual sites. Results show variability in failure probabilities across methods and locations. Sentinel-1-DA generally predicts the lowest P_f, suggesting a more optimistic assessment of failure risk. For instance, at Altenahr-Ahr, P_f is 5% with Sentinel-1-DA, compared to 3% with ESA CCI-DA and 8% with ParFlow-CLM-OL. In contrast, ParFlow-CLM-OL consistently yields higher probabilities, such as 25% at Jünkerath-Kyll and 23% at Opladen-Wupper, indicating a more conservative or higher-risk model.

At some locations, such as Prüm2-Prüm and Prümzurlay-Prüm, the probabilities remain relatively moderate across all methods. However, Opladen-Wupper exhibits high failure probabilities regardless of the method, with P_f reaching 20% (Sentinel-1-DA), 17% (ESA CCI-DA), and 23% (ParFlow-CLM-OL). This variation across locations and methodologies highlights the sensitivity of risk assessment to the data

Table 4 The probability of failure calculated using the FORM. The analysis is based data assimilation accuracy (*DAA*) greater than 0.2 at individual locations: (a) Altenahr-Ahr, (b) Jünkerath-Kyll, (c) Kordel-Kyll, (d) Prüm2-Prüm, (e) Prümzurlay-Prüm, and (f) Opladen-Wupper

	P_f					
	LSF (refer to 3.4.2 section)					
	DAA > 0.2					
	(a)	(b)	(c)	(d)	(e)	(f)
Sentinel-1-DA	5%	10%	9%	7%	9%	20%
ESA CCI-DA	3%	12%	7%	6%	11%	17%
ParFlow-CLM-OL	8%	25%	12%	14%	13%	23%

assimilation approach used and underscores the importance of selecting an appropriate method for reliable hydrological predictions.

The reduction in discharge *RE* observed in this study (e.g., from 5.1% in the open loop to 1.5% with ESA CCI DA at Altenahr-Ahr) is notably lower than those reported in similar hydrological data assimilation studies. Bartholmes et al. (2009), for example, reported forecast accuracy gains of 20–60% in probabilistic flood forecasts using the European Flood Alert System (EFAS), but with higher residual error levels. Similarly, Nguyen et al. (2021) showed Sentinel-1 SM assimilation reduced *RMSE* and improved peak discharge accuracy by up to 30%, which supports the improvements observed here. Moreover, our use of FORM-based probabilistic validation (e.g., P_f = 3–17% for ESA CCI DA) offers a more comprehensive assessment of model reliability than traditional performance metrics such as *RMSE* or *CE*. This approach builds on recent advances by Soltani et al. (2024), who highlighted the importance of probabilistic frameworks in enhancing the credibility of hydrological modeling. Their findings support the integration of ensemble-based soil moisture assimilation with robust risk-based evaluation methods, as demonstrated in this study.

Improved SWC estimations through data assimilation enhance the representation of antecedent hydrological conditions, which are crucial for initializing hydrological models used in flood prediction. More accurate SWC estimates improve the model's ability to capture infiltration, runoff generation, and soil saturation dynamics, leading to more reliable flood forecasts. Additionally, quantifying uncertainties in model outputs enables probabilistic forecasting, which supports risk-based decision-making by providing confidence intervals for predicted flood magnitudes. Incorporating these findings into operational flood forecasting frameworks could enhance early warning systems and improve flood risk assessments by refining precipitation-runoff relationships and threshold exceedance probabilities.

5 Conclusions and Future Perspectives

This study demonstrates the crucial role of advanced data assimilation (DA) methods in enhancing the accuracy of hydrological simulations, particularly for extreme events like the July 2021 floods. By integrating remotely sensed soil moisture data into the ParFlow-CLM hydrological model using a sequential DA approach with the Ensemble Kalman Filter (EnKF), the research effectively addresses key challenges related to uncertainties in peak flow predictions.

The findings show that all data assimilation strategies improve peak discharge predictions compared to the open loop (ParFlow-CLM-OL) simulation, with SWC ESA CCI DA offering the best balance between resolution and accuracy. It consistently delivers lower *RE* and better alignment with observed peak discharge values. While SWC Sentinel-1 DA offers higher spatial resolution, it has slightly higher *RE* but still outperforms the open loop simulation, especially in capturing peak flows.

Additionally, the assimilation of satellite-based data improves extreme flow predictions without significantly altering baseline flow patterns, which explains the minimal variation in correlation coefficients between observed and modeled discharges across different strategies. These enhancements are especially important for flood forecasting, where precise peak discharge predictions are critical for risk assessment and decision-making. This study highlights the importance of integrating high-quality satellite-derived soil moisture data through advanced DA techniques like EnKF to improve the predictive power of hydrological models. Reducing uncertainties and improving the reliability of flood simulations will be pivotal in mitigating the impacts of extreme hydrological events in the future.

Compared to previous hydrological modeling studies (e.g., Naz et al. 2019; Tian et al. 2020), our results demonstrate lower *RE* and P_f values across both soil moisture and discharge simulations, particularly under extreme event conditions. The use of FORM-based probabilistic analysis further differentiates this study by providing a robust, risk-oriented performance evaluation, which has not been widely adopted in comparable research.

Despite the promising results, this study has some limitations that warrant attention. The resampling of satellite soil

moisture data with different spatial resolutions to match the high-resolution hydrological model grid (611 m) introduces important considerations. While Sentinel-1 data, with its finer resolution (1 km), has the potential to capture localized hydrological dynamics, the resampling process, particularly using the First-Order Conservative method, may smooth out high-frequency spatial details, limiting this advantage. Conversely, ESA CCI data, with its coarse resolution (~27 km), inherently lacks spatial detail and, even after downscaling, cannot adequately represent small-scale variability. As a result, the assimilation of such differently scaled data sources can influence the model's capacity to represent local flood dynamics. The performance comparison between Sentinel-1 DA and ESA CCI DA should therefore be interpreted with caution, as resampling may reduce the relative benefit of higher-resolution data in detecting localized hydrological responses. It should also be noted that the GLEAM soil moisture product, used as one of the reference datasets in this study, is itself partly based on ESA CCI observations. This interdependency should be considered when interpreting validation results involving GLEAM.

The Ensemble Kalman Filter (EnKF) used in this study is computationally demanding. Increasing the number of ensemble members can improve the performance of the DA system by better capturing the uncertainty, but it also substantially increases computational cost. This trade-off between performance and efficiency is a critical consideration, especially for operational applications.

The outcomes of this study offer valuable insights for policy and decision-making in the domain of flood risk management. Improved flood peak predictions achieved through satellite data assimilation can significantly enhance the reliability of early warning systems. This, in turn, can support timely evacuation decisions, optimize emergency response, and reduce the overall socio-economic impact of extreme hydrological events. Furthermore, these modeling approaches can be integrated into long-term planning frameworks for resilient infrastructure, land use zoning, and water resource management in flood-prone regions. Incorporating data assimilation frameworks into operational hydrological forecasting platforms can also guide investment in Earth observation technologies and high-performance computing infrastructures. Future collaborations between scientific communities, civil protection agencies, and policymakers will be key to turning these technical improvements into actionable, life-saving outcomes.

For future work, research could focus on several areas to build on the findings of this study. First, expanding the integration of multiple satellite-based data sources (such as higher-resolution datasets or additional remote sensing techniques) could further improve the accuracy and spatial resolution of hydrological models. Additionally, exploring the use of more advanced DA techniques, such as hybrid or machine learning-based methods, could provide a deeper understanding of the uncertainties in hydrological simulations.

Another important avenue for future research would be assessing the performance of the current methods in different geographical regions and hydrological conditions to evaluate their generalizability. Long-term monitoring and validation of these techniques through case studies of other extreme weather events, such as droughts or wildfires, could also help refine the methods for broader applications.

As a direction for future work, we recommend conducting a more systematic sensitivity analysis of key data assimilation parameters, particularly the ensemble size and the assumed observational error within the EnKF framework. In this study, the Ensemble Kalman Filter (EnKF) data assimilation framework was implemented with 50 ensemble members and an assumed observational error of 0.04 m^3/m^3 for soil moisture. These choices were based on a balance between computational efficiency and accuracy, guided by values commonly reported in the literature (Naz et al. 2019; Gebler et al. 2019). However, no dedicated sensitivity analysis was performed to evaluate the impact of these parameters on model performance, particularly regarding peak discharge simulations during the extreme July 2021 flood event. This decision was primarily due to computational constraints, as running the hydrological model with multiple parameter configurations across the full ensemble and assimilation cycles would have significantly increased the computational burden. While previous studies suggest that the chosen parameters are within a reasonable and effective range, future work should include a targeted sensitivity analysis to assess how variations in ensemble size and observational error assumptions might influence the accuracy and robustness of flood predictions.

As a future direction, we also suggest evaluating soil moisture data assimilation across diverse flood events, climates, and hydrological settings. While our results show strong performance for CCI-SM DA, confirming its robustness requires broader testing. Given the central role of antecedent soil moisture in flood generation, we expect the approach to be transferable, but multi-region, multi-event validation is essential.

Supplementary Information The online version contains supplementary material available at https://doi.org/10.1007/s41748-025-00726-8.

Acknowledgements This research was funded by the Deutsche Forschungsgemeinschaft (DFG, German Research Foundation) – Project number: 320397309.

Author Contributions Samira Sadat Soltani: Conceived and designed the study, performed the analysis, and wrote the initial draft of the

manuscript. Alexandre Belleflamme: Providing supports for the simulations, contributed to revising the manuscript critically for important intellectual content and assisted with refining the overall study approach. Klaus Goergen: Provided critical revisions and insightful feedback, helping to enhance the clarity and rigor of the manuscript. Stefan Kollet: Served as the project supervisor, offering guidance and oversight throughout the study and ensuring the integrity and quality of the research, provided critical revisions and insightful feedback.

Funding Open Access funding enabled and organized by Projekt DEAL. We gratefully acknowledge the support of the German Research Foundation (DFG) and Earth System Modelling Project (ESM) for funding this study by providing computing time on the ESM partition of the supercomputer JUWELS at Jülich Supercomputing Centre (JSC).

Data Availability The data and codes supporting this study's findings are available upon a rational request from the corresponding author.

Declaration

Conflict of Interests The authors declare that they have no known competing financial interests or personal relationships that could have appeared to influence the work reported in this paper.

References

Abbaszadeh P, Moradkhani H, Yan H (2018) Enhancing hydrologic data assimilation by evolutionary particle filter and Markov chain Monte Carlo. Adv Water Resour 111:192–204

Abbott M, Bathurst J, Cunge J, O'connell P, Rasmussen J (1986) An introduction to the European hydrological System—Systeme hydrologique european, SHE, 2: structure of a physically-based, distributed modelling system. J Hydrol 87:61–77

AGE: Hochwasserereignis (2021) l'Administration de la gestion de l'eau (AGE), Esch-sur-Alzette, Luxembourg. https://eau.gouvernement.lu/fr/actualites/2021/07-juillet/ Hochwasserereignis2021.html (last access: 9 May 2022), 19 July 2021

Ashby SF, Falgout RD (1996) A parallel multigrid preconditioned conjugate gradient algorithm for groundwater flow simulations. Nucl Sci Eng 124:145–159

Bartholmes JC, Thielen J, Ramos MH, Gentilini S (2009) The European flood alert system EFAS–Part 2: statistical skill assessment of probabilistic and deterministic operational forecasts. Hydrol Earth Syst Sci 13(2):141–153

Bauer-Marschallinger B, Freeman V, Cao S, Paulik C, Schaufler S, Stachl T, Modanesi S, Massari C, Ciabatta L, Brocca L, Wagner W (2018) Toward global soil moisture monitoring with Sentinel-1: Harnessing assets and overcoming Obstacles. IEEE Trans Geosci Remote Sens 1–20. https://doi.org/10.1109/TGRS.2018.2858004

Beck HE, de Jeu RA, Schellekens J, van Dijk AI, Bruijnzeel LA (2009) Improving curve number-based storm runoff estimates using soil moisture proxies. IEEE J Sel Top Appl Earth Observations Remote Sens 2:250–259

Belleflamme A, Goergen K, Wagner N, Kollet S, Bathiany S, El Zohbi J, Rechid D, Vanderborght J, Vereecken H (2023) Hydrological forecasting at impact scale: the integrated parflow hydrological model at 0.6 Km for climate resilient water resource management over Germany. Front Water 5:1183642

BMI: Bericht zur Hochwasserkatastrophe (2021): Katastrophenhilfe, Wiederaufbau und Evaluierungsprozesse, Bundesministerium des 955 Innern und für Heimat, Berlin, Germany. Available: https://www.bmi.bund.de/SharedDocs/downloads/DE/veroeffentlichungen/2022/abschlussbericht-hochwasserkatastrophe.pdf?__blob=publicationFile&v=1 (last access: 9 May 2022), 2022

Brocca L, Melone F, Moramarco T, Singh V (2009) Assimilation of observed soil moisture data in storm rainfall-runoff modeling. J Hydrol Eng 14:153–165

Brocca L, Ciabatta L, Massari C, Camici S, Tarpanelli A (2017) Soil moisture for hydrological applications: open questions and new opportunities. Water 9:140

Chai T, Draxler RR Root mean square error (RMSE) or mean absolute error (MAE)?– Arguments against avoiding RMSE in the literature. Geosci Model Dev, 7, 1247–1250, https://doi.org/10.5194/gmd-7-1247-2014, 2014.

Colliander A, Jackson TJ, Bindlish R, Chan S, Das N, Kim S, Cosh M, Dunbar R, Dang L, Pashaian L (2017) Validation of SMAP surface soil moisture products with core validation sites. Remote Sens Environ 191:215–231

Cornelissen T, Diekkrüger B, Bogena HR (2014) Significance of scale and lower boundary condition in the 3D simulation of hydrological processes and soil moisture variability in a forested headwater catchment. J Hydrol 516:140–153

Corzo G, Solomatine D (2007) Baseflow separation techniques for modular artificial neural network modelling in flow forecasting. Hydrol Sci J 52:491–507

Dai Y, Zeng X, Dickinson RE, Baker I, Bonan GB, Bosilovich MG, Denning AS, Dirmeyer PA, Houser PR, Niu G (2003) The common land model. Bull Am Meteorol Soc 84:1013–1024

Danielson JJ, Gesch DB (2011) Global multi-resolution terrain elevation data 2010 (GMTED2010). US Geological Survey

De Santis D, Biondi D, Crow WT, Camici S, Modanesi S, Brocca L, Massari C (2021) Assimilation of satellite soil moisture products for river flow prediction: an extensive experiment in over 700 catchments throughout Europe. Water Resour Res 57(6):e2021WR029643

Dechant C, Moradkhani H (2011) Radiance data assimilation for operational snow and streamflow forecasting. Adv Water Resour 34:351–364

Dietze M, Bell R, Ozturk U, Cook KL, Andermann C, Beer AR, Damm B, Lucia A, Fauer FS, Nissen KM, Sieg T, Thieken AH (2022) More than heavy rain turning into fast-flowing water±A landscape perspective on the 2021 Eifel floods, EGUsphere [preprint]. https://doi.org/10.5194/egusphere-2022-7

Dorigo W, Wagner W, Albergel C, Albrecht F, Balsamo G, Brocca L, Chung D, Ertl M, Forkel M, Gruber A, Haas E (2017) ESA CCI soil moisture for improved Earth system understanding: State-of-the Art and future directions. Remote Sens Environ 203:185–215

Dottori F, Szewczyk W, Ciscar J-C, Zhao F, Alfieri L, Hirabayashi Y, Bianchi A, Mongelli I, Frieler K, Betts RA (2018) Increased human and economic losses from river flooding with anthropogenic warming. Nat Clim Change 8:781–786

Evensen G (1994) Sequential data assimilation with a nonlinear quasi-geostrophic model using Monte Carlo methods to forecast error statistics. J Geophys Research: Oceans 99:10143–10162
Evensen G (2003) The ensemble Kalman filter: theoretical formulation and practical implementation. Ocean Dyn 53:343–367
Fang Z, Bogena H, Kollet S, Koch J, Vereecken H (2015) Spatio-temporal validation of long-term 3D hydrological simulations of a forested catchment using empirical orthogonal functions and wavelet coherence analysis. J Hydrol 529:1754–1767
Fatichi S, Katul GG, Ivanov VY, Pappas C, Paschalis A, Consolo A, Kim J, Burlando P (2015) Abiotic and biotic controls of soil moisture Spatiotemporal variability and the occurrence of hysteresis. Water Resour Res 51:3505–3524
Fekete A, Sandholz S (2021) Here comes the flood, but not failure? Lessons to learn after the heavy rain and pluvial floods in Germany 2021. Water 13:3016. https://doi.org/10.3390/w13213016
Frei S, Fleckenstein J, Kollet S, Maxwell RM (2009) Patterns and dynamics of river–aquifer exchange with variably-saturated flow using a fully-coupled model. J Hydrol 375:383–393
Gebler S, Kurtz W, Pauwels V, Kollet S, Vereecken H, Franssen H (2019) Assimilation of high-resolution soil moisture data into an integrated terrestrial model for a small-scale head-water catchment. Water Resour Res 55:10358–10385
Harmel RD, Smith PK (2007) Consideration of measurement uncertainty in the evaluation of goodness-of-fit in hydrologic and water quality modeling. J Hydrol 337:326–336
Hengl T, Mendes de Jesus J, Heuvelink GBM, Gonzalez R, Kilibarda M, Blagotic M, A., et al (2017) SoilGrids250m: global gridded soil information based on machine learning. PLoS ONE 12:e0169748. https://doi.org/10.1371/journal.pone.0169748
Herbst M, Diekkrüger B, Vanderborght J (2006) Numerical experiments on the sensitivity of runoff generation to the Spatial variation of soil hydraulic properties. J Hydrol 326:43–58
Hersbach H, Bell B, Berrisford P, Hirahara S, Horányi A, Muñoz-Sabater J, Nicolas J, Peubey C, Radu R, Schepers D, Simmons A (2020) The ERA5 global reanalysis. Q J R Meteorol Soc 146(730):1999–2049
Houtekamer PL, Mitchell HL (1998) Data assimilation using an ensemble Kalman filter technique. Mon Weather Rev 126(3):796–811
Ivanov VY, Fatichi S, Jenerette GD, Espeleta JF, Troch PA, Huxman TE (2010) Hysteresis of soil moisture Spatial heterogeneity and the homogenizing effect of vegetation. Water Resour Res, 46
Jones PW (1999) First-and second-order Conservative remapping schemes for grids in spherical coordinates. Mon Weather Rev 127(9):2204–2210
Junghänel T, Bissolli P, Daßler J, Fleckenstein R, Imbery F, Janssen W, Kaspar F, Lengfeld K, Leppelt T, Rauthe M, Rauthe-Schöch A, Rocek M, Walawender E, Weigl E Hydro-klimatologische Einordnung der Stark- und Dauerniederschläge in Teilen Deutschlands im Zusammenhang mit dem Tiefdruckgebiet Bernd vom 12. bis 19. Juli 2021, DWD– Deutscher Wetterdienst, Offenbach, Germany. https://www.dwd.de/DE/leistungen/besondereereignisse/niederschlag/20210721_bericht_starkniederschlaege_tief_bernd.html (last access: 9 May 2022), 22 July 2021
Kohler MA, Linsley RK (1951) Predicting the runoff from storm rainfall, vol 30. US Department of Commerce, Weather Bureau
Kollet SJ (2009) Influence of soil heterogeneity on evapotranspiration under shallow water table conditions: transient, stochastic simulations. Environ Res Lett 4:035007
Kollet SJ, Maxwell RM (2006) Integrated surface–groundwater flow modeling: A free-surface overland flow boundary condition in a parallel groundwater flow model. Adv Water Resour 29:945–958
Kuffour BN, Engdahl NB, Woodward CS, Condon LE, Kollet S, Maxwell RM (2020) Simulating coupled surface–subsurface flows with parflow v3. 5.0: capabilities, applications, and ongoing development of an open-source, massively parallel, integrated hydrologic model. Geosci Model Dev 13:1373–1397
Legates DR, McCabe Jr GJ (1999) Evaluating the use of goodness-of-fit measures in hydrologic and hydroclimatic model validation. Water Resour Res 35:233–241
Lenderink G, Van Meijgaard E (2010) Linking increases in hourly precipitation extremes to atmospheric temperature and moisture changes. Environ Res Lett 5(2):025208
Lenderink G, Ban N, Brisson E, Berthou S, Cortés-Hernández VE, Kendon E, Fowler HJ, de Vries H (2025) Are dependencies of extreme rainfall on humidity more reliable in convection-permitting climate models? Hydrol Earth Syst Sci 29(4):1201–1220
Li Y, Ryu D, Western AW, Wang Q (2013) Assimilation of stream discharge for flood forecasting: the benefits of accounting for routing time lags. Water Resour Res 49:1887–1900
Lievens H, Reichle RH, Liu Q, De Lannoy GJ, Dunbar RS, Kim S, Das NN, Cosh M, Walker JP, Wagner W (2017) Joint Sentinel-1 and SMAP data assimilation to improve soil moisture estimates. Geophys Res Lett 44:6145–6153
Liu PL, Der Kiureghian A (1991) Optimization algorithms for structural reliability. Struct Saf 9(3):161–177
Liu YY, Parinussa R, Dorigo WA, De Jeu RA, Wagner W, Van Dijk A, McCabe MF, Evans J (2011) Developing an improved soil moisture dataset by blending passive and active microwave satellite-based retrievals. Hydrol Earth Syst Sci 15:425–436
Liu Y, Weerts A, Clark M, Franssen H, Kumar H-J, Moradkhani S, Seo H, Schwanenberg D-J, Smith D, P., and, Van Dijk A (2012) Advancing data assimilation in operational hydrologic forecasting: progresses, challenges, and emerging opportunities. Hydrol Earth Syst Sci 16:3863–3887
Long D, Longuevergne L, Scanlon BR (2014) Uncertainty in evapotranspiration from land surface modeling, remote sensing, and GRACE satellites. Water Resour Res 50:1131–1151
Madsen HO, Krenk S, Lind NC (2006) Methods of structural safety, Courier Corporation
Maina FZ, Siirila-Woodburn ER, Vahmani P (2020) Sensitivity of meteorological-forcing resolution on hydrologic variables. Hydrol Earth Syst Sci 24:3451–3474
Matgen P, Montanari M, Hostache R, Pfister L, Hoffmann L, Plaza D, Pauwels V, De Lannoy G, De Keyser R, Savenije H (2010) Towards the sequential assimilation of SAR-derived water stages into hydraulic models using the particle filter: proof of concept. Hydrol Earth Syst Sci 14:1773–1785
Maxwell RM, Kollet SJ (2008) Interdependence of groundwater dynamics and land-energy feedbacks under climate change. Nat Geosci 1:665–669
Maxwell RM, Miller NL (2005) Development of a coupled land surface and groundwater model. J Hydrometeorol 6:233–247
Maxwell RM, Kollet SJ, Smith SG, Woodward CS, Falgout RD, Ferguson IM, Baldwin C, Bosl WJ, Hornung R, Ashby S (2009) ParFlow user's manual. Int Ground Water Model Cent Rep GWMI 1:129
Maxwell RM, Lundquist JK, Mirocha JD, Smith SG, Woodward CS, Tompson AF (2011) Development of a coupled groundwater–atmosphere model. Mon Weather Rev 139:96–116
McMillan H, Hreinsson E, Clark M, Singh S, Zammit C, Uddstrom M (2013) Operational hydrological data assimilation with the recursive ensemble Kalman filter. Hydrol Earth Syst Sci 17:21–38
media-information/2022 /natural-disaster-losses-2021.html, last access: 9 May 2022
Miralles DG, Holmes TR, De Jeu RA, Gash JH, Meesters AG, Dolman AJ (2011) Global land-surface evaporation estimated from satellite-based observations. Hydrol Earth Syst Sci 15(2):453–469
Mohr S, Ehret U, Kunz M, Ludwig P, Caldas-Alvarez A, Daniell JE, Ehmele F, Feldmann H, Franca MJ, Gattke C (2022) A multi-disciplinary analysis of the exceptional flood event of July 2021

in central Europe. Part 1: Event description and analysis, Natural Hazards and Earth System Sciences Discussions, 1–44, 2022
Moradkhani H, Sorooshian S, Gupta HV, Houser PR (2005) Dual state–parameter Estimation of hydrological models using ensemble Kalman filter. Adv Water Resour 28:135–147
Moriasi DN, Arnold JG, Van Liew MW, Bingner RL, Harmel RD, Veith TL (2007) Model evaluation guidelines for systematic quantification of accuracy in watershed simulations. Trans ASABE 50:885–900
Munich Re Hurricanes, cold waves, tornadoes: weather disasters in USA dominate natural disaster losses in 2021– Europe: extreme flash floods with record losses, Munich re, Media relations on 10 January 2022: natural disaster losses 2021, Munich, Germany, https://www.munichre.com/en/company/media-relations/media-information-and-corporate-news/
Myhre G, Alterskjær K, Stjern CW, Hodnebrog Ø, Marelle L, Samset BH, Sillmann J, Schaller N, Fischer E, Schulz M, Stohl A (2019) Frequency of extreme precipitation increases extensively with event rareness under global warming. Sci Rep 9(1):16063
Nash JE, Sutcliffe JV (1970) River flow forecasting through conceptual models' part I—A discussion of principles. J Hydrol 10:282–290
Naz BS, Kurtz W, Montzka C, Sharples W, Goergen K, Keune J, Gao H, Springer A, Franssen H, H.-J., and, Kollet S (2019) Improving soil moisture and runoff simulations at 3 Km over Europe using land surface data assimilation. Hydrol Earth Syst Sci 23:277–301
Nguyen TH, Ricci S, Fatras C, Piacentini A, Delmotte A, Lavergne E, Kettig P (2021) Improvement of Flood Extent Representation with Remote Sensing Data and Data Assimilation Applied to Hydrodynamic Numerical Models. Electrical Engineering and Systems Science. Sep 17
Nie S, Zhu J, Luo Y (2011) Simultaneous Estimation of land surface scheme States and parameters using the ensemble Kalman filter: identical twin experiments. Hydrol Earth Syst Sci 15:2437–2457
Nissen KM, Ulbrich U (2017) Increasing frequencies and changing characteristics of heavy precipitation events threatening infrastructure in Europe under climate change. Nat Hazards Earth Syst Sci 17:1177–1190
Papaioannou I, Straub D (2021) Variance-based reliability sensitivity analysis and the FORM α-factors. Reliab Eng Syst Saf 210:107496
Poméon T, Wagner N, Furusho C, Kollet S, Reinoso-Rondinel R (2020) Performance of a PDE-based hydrologic model in a flash flood modeling framework in sparsely-gauged catchments. Water 12:2157
Rackwitz R, Fiessler B (1979) Structural reliability under combined random load s quences. Comput Struct 9(5):489–494
Reichle RH, McLaughlin DB, Entekhabi D (2002) Hydrologic data assimilation with the ensemble Kalman filter. Mon Weather Rev 130:103–114
Saadi M, Furusho-Percot C, Belleflamme A, Chen J-Y, Trömel S, Kollet S (2023a) How uncertain are precipitation and peak flow estimates for the July 2021 flooding event? Nat Hazards Earth Syst Sci 23:159–177
Saadi M, Furusho-Percot C, Belleflamme A, Trömel S, Kollet S, Reinoso-Rondinel R (2023b) Comparison of three radar-based precipitation nowcasts for the extreme July 2021 flooding event in Germany. J Hydrometeorol 24:1241–1261
Sahoo AK, Pan M, Troy TJ, Vinukollu RK, Sheffield J, Wood EF (2011) Reconciling the global terrestrial water budget using satellite remote sensing. Remote Sens Environ 115:1850–1865
Schröter K, Kunz M, Elmer F, Mühr B, Merz B (2015) What made the June 2013 flood in Germany an exceptional event? A hydrometeorological evaluation. Hydrol Earth Syst Sci 19:309–327
Shrestha P, Sulis M, Masbou M, Kollet S, Simmer C (2014) A scale-consistent terrestrial systems modeling platform based on COSMO, CLM, and ParFlow. Monthly Weather Rev 142:3466–3483
Soltani S (2022) Assimilating remote sensing information into a distributed hydrological model for improving water budget predictions. Université de Strasbourg; Sharif University of Technology (Tehran)
Soltani SS (2025) 2 assimilating GRACE data. Remote Sensing for Geophysicists, p 21
Soltani SS, Ataie-Ashtiani B, Danesh-Yazdi M, Simmons CT (2020) A probabilistic framework for water budget Estimation in low runoff regions: A case study of the central basin of Iran. J Hydrol 586:124898
Soltani SS, Ataie-Ashtiani B, Simmons CT (2021) Review of assimilating GRACE terrestrial water storage data into hydrological models: advances, challenges and opportunities. Earth Sci Rev 213:103487
Soltani SS, Fahs M, Al Bitar A, Ataie-Ashtiani B (2022a) Improvement of soil moisture and groundwater level estimations using a scale-consistent river parameterization for the coupled ParFlow-CLM hydrological model: A case study of the upper rhine basin. J Hydrol 610:127991
Soltani SS, Fahs M, Bitar A, A., and, Ataie-Ashtiani B (2022b) Fully coupled subsurface-land surface hydrological models: A scaling approach to improve subsurface storage predictions, Copernicus Meetings
Soltani SS, Ataie-Ashtiani B, Bitar A, Simmons A, Younes CT, A. and, Fahs M (2024) Assimilating multivariate remote sensing data into a fully coupled subsurface-land surface hydrological model. Journal of Hydrology, 641, p.131812
Soltani S, Belleflamme A, Hammoudeh S, Kollet S (2025) Enhancing Streamflow Predictions with a River Parameterization in an Integrated Hydrological Model, EGU General Assembly 2025, Vienna, Austria, 27 Apr–2 May 2025, EGU25-11292. https://doi.org/10.5194/egusphere-egu25-11292
Tian S, Renzullo LJ, Pipunic RC, Lerat J, Sharples W, Donnelly C (2020) Satellite soil moisture data assimilation for improved operational continental water balance prediction. Hydrology and Earth System Sciences Discussions.; 2020:1–26
Tramblay Y, Bouvier C, Martin C, Didon-Lescot J-F, Todorovik D, Domergue J-M (2010) Assessment of initial soil moisture conditions for event-based rainfall–runoff modelling. J Hydrol 387:176–187
Tramblay Y, Bouvier C, Ayral P-A, Marchandise A (2011) Impact of rainfall Spatial distribution on rainfall-runoff modelling efficiency and initial soil moisture conditions Estimation. Nat Hazards Earth Syst Sci 11:157–170
Tramblay Y, Bouaicha R, Brocca L, Dorigo W, Bouvier C, Camici S, Servat É (2012) Estimation of antecedent wetness conditions for flood modelling in Northern Morocco. Hydrol Earth Syst Sci 16:4375–4386
Trenberth KE (2011) Changes in precipitation with climate change. Climate Res 47:123–138
Van Genuchten MT (1980) A closed-form equation for predicting the hydraulic conductivity of unsaturated soils. Soil Sci Soc Am J 44:892–898
Wagner W, Hahn S, Kidd R, Melzer T, Bartalis Z, Hasenauer S, Figa J, De Rosnay P, Jann A, Schneider S (2013) The ASCAT soil moisture product: A review of its. Meteorol Z 22:1–29
Wang D, Chen Y, Cai X (2009) State and parameter Estimation of hydrologic models using the constrained ensemble Kalman filter. Water Resour Res, 45(11)
Westra S, Alexander LV, Zwiers FW (2013) Global increasing trends in annual maximum daily precipitation. J Clim 26(11):3904–3918
Willmott CJ (1981) On the validation of models. Phys Geogr 2:184–194